Nuclear Magnetic Resonance and Relaxation in Ferromagnetic Heavy Rare Earth Metals: Terbium and Dysprosium

by

Naokatsu Sano

Osaka University

Graduated School of Engineering Science

Toyonaka, Osaka

February 1971

TABLE OF CONTENTS

PART I. Nuclear Magnetic Resonance and Relaxation of ^{163}Dy in Ferromagnetic Dysprosium Metal

TABLE OF CONTENTS (continued)

PART II. Nuclear Magnetic Resonance and Relaxation of ^{159}Tb in Ferromagnetic Terbium Metal

PART I

Nuclear Magnetic Resonance and Relaxation of ^{163}Dy in Ferromagnetic Dysprosium Metal

Abstract.

Nuclear magnetic resonance and relaxation phenomena of ^{163}Dy have been investigated by spin echo technique at liquid helium temperatures. The nuclear magnetic resonance spectrum consists of five equally spaced lined in the frequency range from 300MHz to 2000MHz. The center line frequency corresponding to the Zeeman energy is 1162MHz and the frequency difference of the adjacent lines corresponding to the quadrupolar effects is 409MHz. The spin-lattice relaxation decay law was found to be non-exponential. A theory that accounts for the observed spin-lattice relaxation is presented. It is concluded that a process in which the nuclear energy relaxes to the kinetic energy of the conduction electrons via spin waves is predominant in the spin-lattice relaxation, and the spin-spin relaxation time is solely determined by the spin-lattice relaxation.

I. Introduction

In heavy rare earth metals, trivalent rare earth ions are embedded in a sea of conduction electrons. The unfilled 4f electrons in the trivalent ions are closely bound inside the outer closed shells and at each lattice site there is left a highly localized magnetic moment due to these 4f electrons. The moment is quite well given by the application of Hund's rule so that J, the total spin plus orbital angular momentum is treated as a good quantum number. Thus in heavy rare earth metals, the localized magnetic electrons carry the major part of the bulk magnetic moment and itinerant conduction electrons contribute little magnetic moment. The conduction electrons enter into the magnetic properties primarily as a coupling mechanisms between localized 4f electrons through sf exchange interactions.

The unquenched orbital angular momentum of the unfilled 4f electrons provides very large hyperfine magnetic field in heavy rare earth metals. At the same time, large electric quadrupole hyperfine energy is produced. Bleaney first discussed the hyperfine interactions in rare earth metals in detail.[1)] Also there exist various other origins to produce hyperfine energy; that is, the conduction electron polarization, the core polarization, electric field gradient produced by non-cubic nature of the lattice, electric field gradient produced by the conduction electrons and so on. These contributions are usually very small, except in Gd metal in which the trivalent ions are in S-state.

The measurements of the hyperfine interaction in heavy rare earth metals have been done by nuclear specific heat

measurements[2] and Mössbauer studies[3] in the past. But the accuracy of the measurements is not so good in both methods and for detailed study of the hyperfine interactions it is hoped to do NMR experiment in these metals. Herve and Veillet[4] made a preliminary measurement of NMR in terbium metal, but their signal was not well reproducible and could not be ascribed with certainty to NMR of terbium metal.

Because of the large hyperfine energy, the NMR frequency in magnetically ordered state in these metals is expected in frequency range between a few hundred MHz and several GHz. We developed spin echo apparata covering this frequency range and first observed the spin echo NMR signals in Dy[5] and Tb[6] metals and in alloys[7] formed by solid solution of rare earth metals, and obtained precise values of the magnetic and electric quadrupole hyperfine energies. The observed values are nearly in agreement with those calculated by Bleaney[1] and independently by Kondo[8] for the hyperfine energies arising from the unfilled 4f electrons.

In our previous report,[9] we discussed the hyperfine interaction between the conduction electrons and the nuclei, and also we made a preliminary measurement of the nuclear relaxation times in ferromagnetic Dy metal. On the other hand Gill and Kaplan[10] measured the tail mode of the recovery curves for some lines of Dy^{161} and Dy^{163} also in ferromagnetic phase, by means of a saturating comb method. However, detailed discussions on the hyperfine energy and the relaxation mechanism have not yet been given.

In this report, we shall present details of NMR measurements of Dy^{163} in ferromagnetic Dy metal at low temperatures. Dy metal

is normal ferromagnetic below about 85°K in which the easy axis of the magnetization is along $\langle 11\bar{2}0 \rangle$ in the c-plane.[11] Our main concern is the relaxation mechanism in Dy metal.[12] Because of large electric quadrupole energy, the NMR lines of Dy^{163} in ferromagnetic Dy metal split into five well separated lines, and the nuclear relaxation does not follow a simple exponential curve but follows a composition of five exponentail functions. We measured the relaxation decay in detail and analysed the decay curve by the use of a theoretical formula obtained by solving rate equations, and discuss what is the main origin in the relaxation. The Weger's mechanism, that is, the relaxation of nuclear spin energy to the kinetic energy of the conduction electrons via spin waves through hyperfine interactions of the 4f electrons and sf exchange interactions, which was proposed first for 3d ferromagnetic metals,[13] is found to be the main origin of the relalaxation in Dy metal. Also spin-spin relaxation was measured and it will be shown that Walstedt mechanism,[14] that is, the contribution of spin lattice relaxation to spin-spin relaxation, is the main origin of T_2. Our previous preliminary results[9] on the relaxation were too inaccurate and the relaxation mechanism proposed at that time is not good. Also the result to be presented in this paper is not in agreement with that of Gill and Kaplan.[10]

For the discussion of the relaxation, it is necessary to know the details of the hyperfine interactions, and the contributions to the hyperfine energies from other origins than the unfilled 4f electrons will be discussed in some details.

In II the experimental method used in the present measurement will be described and in III the experimental results of the resonance frequencies, line shapes, and spin-lattice and spin-spin relaxations will be presented. The theory of the relaxation will be given in IV. The discussion of the results together with numerical estimation of the relaxation probabilities will be offered in V. The solution of the rate equations which describes the decay behavious in the case of quadrupole split NMR lines will be given in Appendix.

II. Experimental procedure

In the present studies, Dy metal samples from two commercial sources were used. There was no difference in the results of NMR measurements for both samples. The results presented in next section were obtained with the sample from Materials Research Corporation. According to the supplier, the purity is better than 99.8 per cent and principal impurities are (in per cent), Ho 0.03, Ca 0.02, Tb 0.01, Y 0.01, Sm 0.01, Tm $<$0.01, Gd $<$0.01, Er 0.005, Mg 0.005 and Fe 0.005. Samples used in the NMR measurement were prepared by filing the ignot metal into powder form with a few tens microns in diameter. No care was paid to avoid oxidization and the powders probably were covered with oxide, by which each powder is electrically insulated from others. The powder samples were stored in a descicator and the NMR signals obtained at considerably later days from the filing gave the same frequency and shape as compared to those obtained just after the filing, indicating that there was no trouble about sample treatment. Only a short annealing of the powders was done in an argon atmosphere

to minimize crystal defects.

The spin echo apparatus in ultra high frequency (UHF) range is in principle the same as that of conventional pulse spectrometer. A light house tube was used as an oscillator and coaxial cavities were used as resonant circuits. The echo signal was mixed with a rf wave generated by a Klystron (or a triod tube) local oscillator and the beat at 60 MHz was amplified by an IF amplifier and the detected signal was displayed on an oscilloscope. To cover the whole frequency range of Dy^{163} NMR, several sets of the oscillators and mixers were used. The duration of the rf pulses was fixed at about one microsecond and the amplitude of rf pulses was varied to get optimum intensity of the signal. In some cases at higher frequencies, the power of the oscillator was not sufficient to produce an optimum intensity of the signal and in those cases maximum output of the oscillator was used for the measurement of echo. The signal intensity was quite strong and in best cases the signal-to-noise ratio was better than 10^3.

The line shapes of Dy NMR were determined by point to point plots of the echo intensities when the frequency of the rf pulses was varied with every one or two MHz step. In each one measurement of the echo height it was necessary to adjust the frequencies of the oscillators and the resonance condition of cavity resonators. In narrow frequency range the measurement of relative intensities of echos was reliable, but because the calibration of the sensitivity of the apparatus was quite difficult in widely different frequency ranges the relative intensities of different lines could not be obtained in any accuracy.

The spin-lattice relaxation was measured by stimulated echo method.[15] Because the spectrum consists of five lines in Dy^{163}, which distribute in wide frequency range, only one line can be disturbed by a rf pulse. As will be discussed in next section, the relaxation decay is not simply exponential in this case, and the whole decay curve had to be measured to analyse it to compare with the theory. For this purpose, the stimulated echo method seems to be the best. Because of broad line shape, it was impossible to disturb whole spins belonging to one line by a rf pulse of single frequency, but only a hot spot will be produced at the frequency of the pulse. The observed decay corresponds to the decay of this hot spot. Another method was used to measure the relaxation, namely the four pulses method or the measurement of the echo intensity after a preceding echo. In this method the recovery to the thermal equilibrium is measured and only a portion of the relaxation curve can be obtained with some accuracy. As far as this portion is concerned, the relaxtion curve agreed with that obtained by the stimulated echo method.

The spin-spin relaxation was measured by the change of the echo height when the separation time of two rf pulses which produce the echo was varied. Because the spin-spin relaxation time is very short, the accurate determination of T_2 was rather difficult.

The natural abundances of isotopes of Dy which have magnetic moment are 18.73% for Dy^{161} and 24.97% for Dy^{163}. Both have spin 5/2. Accurate measurement of the relaxation was made only for abundant isotope Dy^{163}. The measurement was done at liquid helium temperatures between 1.4°K and 4.2°K.

The temperature was controlled by regurating pumping rate of helium gas in Dewar vessel. Because the intensities of rf pulses were strong and the relaxation rate is a function of temperature, care was taken to keep good thermal contact between the sample and the helium liquid; powder sample contained in an open glass tube was directly immersed in liquid helium. In superfluid temperature region, liquid helium certainly made direct contact with each fine powder to keep good thermal contact.

III. Experimental results

III 1. The resonance frequency, the line shape, and the enhancement factor.

The observed spectra of Dy^{163} NMR in ferromagnetic Dy metal consist of five lines. In the case of Dy^{161}, the lowest frequency line expected at about 60 MHz is still missing, but other feature is quite the same as that of Dy^{163}. The resonance frequencies are shown in Table I. The spacings between each adjacent lines are all the same within the experimental errors. This means that the NMR spectra consist of lines split by a nuclear electric quadrupole interaction whose principal axis coinsides with the direction of the internal field. The frequency of the center line, corresponds to the Zeeman frequency and the frequency difference, ν_Q, of the adjacent lines, corresponds to $3e^2qQ/2I(2I-1)$, where q is the principal value of the field gradient tensor, Q the nuclear quadrupole moment and I the nuclear spin. In the case of Dy^{163}, the Zeeman frequency is 1162 MHz and ν_Q is 409 MHz, and in the case of Dy^{161}, the Zeeman frequency is 830 MHz and ν_Q

is 386 MHz.

The large magnetic and electric quadrupole hyperfine energies of Dy^{163} in ferromagnetic Dy metal are mainly due to the hyperfine interaction arising from the unfilled 4f electrons of Dy^{+3} ions in the metal. The 4f hyperfine energies were calculated independently by Bleaney[1] and Kondo[8]. Though the numerical values obtained by their theoretical calculations are only rough due to unknown values of various parameters, the calculated values are in agreement with the observed values. The published values of hyperfine energies measured by Mössbauer method[3] also agree with our more precise values.

There are other possible contributions to the hyperfine energies arising from various origins. Namely, for magnetic hyperfine energy, (there are) contributions from the polarization of the conduction electrons and the core polarization. The contribution from the core polarization was estimated by Bleaney[1] and by Freeman and Watson[16] to be $-(g_J-1)J\times 90$ Koe where g_J is the Landé factor and J is the total angular momentum of the unfilled 4f shell ($(g_J-1)J$ is the component of the spin of the 4f shell along the direction of J). For Dy, this core polarization field is about -200 Koe and is quite negligible compared with the observed field (about 6000 Koe). Also the contribution to the magnetic hyperfine field from the polarization of the conduction electrons was estimated from our previous measurement[9] of the change of the resonance frequencies of Dy in Dy metal, Dy-Gd and Dy-Tb alloys to be about -270 Koe*, which too is quite small as compared with the 4f contribution. The hyperfine field due to the

polarization of the conduction electrons will be discussed again in later section in connection with the spin-lattice relaxation. Dipolar and orbital contributions of the conduction electrons to the magnetic hyperfine field may be even smaller than the contribution from the polarization.

---

* Here an uniform polarization model is assumed for the spins of the conduction electrons which is supported by the experimental fact that the line broadening does not change appreciably by alloying. From the analysis of the experimental results, the internal field at Dy nucleus in these alloys or in Dy metal was found to be given by $-110\langle S\rangle$ Koe, where $\langle S\rangle$ is the average value of the spins of the 4f shell over all constituent atoms. In pure Dy metal, $\langle S\rangle$ is 5/2 and the hyperfine field due to the polarization of the conduction electron is estimated to be about -270 Koe.

Some possible contributions to the electric field gradient (EFG) arise from the surrounding Dy ions forming the lattice and also from the non-s character of the conduction electrons. These contributions seem very difficult to be estimated in Dy metal. But in Tm metal in paramagnetic phase, Uhrich and Barnes[17] obtained these contributions from their Mössbauer measurement; namely, they obtained $q_{zz}^{(ce)} = 2.14 \times 10^{24}$ cm^{-3} and $q_{zz}^{(lattice)} = 1.45 \times 10^{24}$ cm^{-3}, where $q_{zz}^{(ce)}$ is the principal value of EFG due to the conduction electrons and $q_{zz}^{(lattice)}$ is that due to the lattice including the Sternheimer coefficient. Here the z-axis is parallel to the c-axis. Though these values are not measured in Dy metal, they may be of about the

same magnitudes in Dy metal as in Tm metal. In Dy metal, this z-axis is perpendicular to the easy direction of the magnetization. On the other hand, the EFG arising from the 4f shell is estimated to be $q^{(4f)} = 35 \times 10^{24}$ cm^{-3} assuming the shielding factor of the close shell electrons to be about 0.2. Thus the contribution from the 4f shell is the main part also in EFG.

From the results for Dy^{161} and Dy^{163}, the ratios of the magnetic dipole and electric quadrupole moments of these two isotopes are determined as $\mu^{163}/\mu^{161} = 1.40 \pm 1\%$ and $Q^{163}/Q^{161} = 1.60 \pm 1\%$.

The shapes of the resonance lines of Dy^{163} are shown in Fig.1. The principal feature of the line shapes is that the center line corresponding to the transition $1/2 \leftrightarrow -1/2$ is the narrowest and the farther satellite lines are the broader. Even the width of the center line is much broader than that expected from spin-spin relaxation. This extra width may probably arise from small fluctuations of the values of the internal field by some imperfections of the crystal. The broader width of the satellite lines than that of the center line may be caused by the fluctuations of the electric field gradient due to similar imperfections. These small fluctuations of the electric field gradient have no effect on the width of the center line. This extra broadening of the resonance lines is quite inhomogeneous in nature. By this inhomogeneity, the observed spin-lattice relaxation corresponds to the relaxation of a hot spot produced by the pulsed rf field. The same situation holds for the observed spin-spin relaxation.

Next, the enhancement of NMR will be discussed briefly. Because the measurement of the power of the rf pulses was not done, we could not determine accurate value of the enhancement factor in Dy metal. But it was clear that the enhancement factor of NMR in Dy metal is very much smaller than that of the resonance in ferromagnetic Fe and Co metals in zero applied field. Probably, the enhancement factor in Dy metal is of the same order of that of domain resonance in Fe or Co metal. Further, some measurements of NMR in external magnetic field were done for Dy metal, and it was found that the decrease of the intensity of the echo with the increase of the applied field was much slower than that in Co metal. Also the rate of the relaxation did not change appreciably even when a weak magnetic field is applied. These facts suggest that there is little wall enhancement in Dy metal and the observed signal corresponds to the resonance of Dy nuclei mainly in bulk domain, contrary to the case of Fe, Co and Ni metals in which wall enhancement is very large and the resonance from nuclei in wall is predominant in zero applied field.

III 2. The spin-lattice relaxation.

Fig.2 shows the decay curves of the stimulated echo amplitudes for all five resonance lines of Dy^{163} in ferromagnetic Dy metal plotted against the time interval between the second and third pulses, at 1.4°K. The decay curve of the resonance line at 1162 MHz was measured also at 4.2°K. As shown in Fig.3, the decay curve measured at 4.2°K coincides exactly with that measured at 1.4°K when the intensities of the stimulated echos are plotted against tT (t is the time interval between the second and third pulses and T is the absolute

temperature). This result indicates that the spin-lattice relaxation probability is proportional to absolute temperature. Though only a hot spot produced by the rf pulses was observed in our experiment, this proportionality to the absolute temperature suggests that the effect of the spectral diffusion is quite negligible, because the latter effect should be independent of temperature. The negligible contribution of the diffusion to the observed spin-lattice relaxation was also checked experimentally: The amplitude of the stimulated echo signal was found to remain constant even when the time interval of the first and second pulses was varied.[15] The smallness of the spectral diffusion comes from the inhomogeneity of the resonance line; the resonance line is not only macroscopically inhomogeneous but also is microscopically inhomogeneous. A discussion will be given again in V,2 in connection with the spin-spin relaxation.

Each decay curve shown in Fig.2 is not simply exponential. This is the feature of the relaxation of NMR lines split by quadrupole interaction. Several authors[18] have discussed the shape of decay curves in this case. The decay curve is the sum of five exponential curves when I=5/2. The time constant of each exponential function can be calculated by solving rate equations for the occupation probabilities of nuclear levels, and depends upon what is the dominant relaxation mechanism. In Appendix, we show the solution of the rate equations for three cases. In all cases, the relaxation probability $W_{m,m'}$ between the nuclear levels m and m' is assumed to be proportional to $|(m|I_x|m')|^2$, where I_x is the component of the nuclear spin perpendicular to the

direction of the internal field, and hence $W_{m,m'}$'s are non zero only when $m' = m \pm 1$. Case A corresponds to the case when $W_{m,m\pm1}$ is independent of $\omega_{m,m\pm1}$. This describes the relaxation decay when the Korringa's mechanism[19] is predominant. Case B shows the case when $W_{m,m\pm1}$ is proportional to $\omega^2_{m,m\pm1}$ corresponding to the relaxation in which the Weger's mechanism[13] is predominant. Case C shows the case when $W_{m,m\pm1}$ is proportional to $\omega^4_{m,m\pm1}$ corresponding to the case when the magneto-elastic coupling contributes mainly to the relaxation. Dependence of $W_{m,m\pm1}$ on $\omega_{m,m\pm1}$ in these mechanisms will be discussed in later section. In all these cases, the decay curves for the stimulated echo signals are calculated theoretically in Appendix, and are shown in Figs. 7, 8 and 9. In calculating decay curves, only one parameter is needed, and we take $W_{3/2,5/2}$ which is the relaxation probability between two lowest energy levels as this unknown parameter.

We compare the observed relaxation decay curves with those shown in Figs. 7, 8 and 9 and it is found that curves shown in Fig.8 agree with the observed curves shown in Fig.2 quite satisfactorily when an appropriate value of the parameter is assumed. Because $W_{m,m\pm1}$ is proportional to absolute temperature T, we take W_o which is equal to $W_{3/2,5/2}/T$ as the parameter instead of $W_{3/2,5/2}$ itself. Taking a value 4.76×10^2 $sec^{-1} \cdot K^{-1}$ for W_o, calculated decay curves of the stimulated echo signals are drawn in Fig.2 with solid curves, which fit the experimental plots quite well. Thus it was found that the spin-lattice relaxation probability $W_{m,m\pm1}$ is proportional to $\left|(m|I_x|m\pm1)\right|^2 \omega^2_{m,m\pm1}$ T. In next section, the Weger's mechanism which gives these frequency and

temperature dependences will be discussed.

III 3. Spin-spin relaxation.

The measurement of the spin-spin relaxation time, T_2, was done for the resonance line at 1162 MHz which corresponds to the transition between 1/2 and -1/2 levels. The height of the spin echo signal was measured by varying the time interval between two pulses necessary to produce the echo, and the decay curves of the echo height is plotted against the twice of this time interval. Contrary to the case of spin-lattice relaxation, it was found that the spin-spin relaxation follows a simple exponential function and T_2 is determined as the decay time of this exponential function, $\exp(-t/T_2)$. We have measured the temperature dependence of T_2 in liquid helium temperature range and the result is shown in Fig.4. Because of fast decay, the accurate determination of T_2 was rather difficult and the measured values of T_2 fluctuate for different series of measurements. Circular plots shown in Fig.4 are the average values of repeated measurements at the same temperature and the virtical line at each plot indicates a probable error.

Fig.4 shows that T_2 is proportional to 1/T. Because the spin-spin relaxation arising from Suhl-Nakamura interaction[20] is generally independent of temperature, and also that the spin-lattice relaxation probability $W_{m,m\pm1}$ is found to be proportional to T as already described this result suggests that T_2 is determined solely by spin-lattice relaxation. The values of T_2 were also measured for other NMR lines though not so accurately. A general trend of the variation of T_2

against the resonance frequency of NMR lines, is that the smaller $\omega_{m,m\pm1}$ is the longer T_2 is. This also agrees with the conclusion of the Walstedt's mechanism[14] for T_2, which gives the contribution of the spin-lattice relaxation to T_2, as will be discussed in later sections.

IV. Theory of the relaxation of Dy nuclear spin in Dy metal.

IV 1. The spin-lattice relaxation mechanisms.

The nuclear spin-lattice relaxation rate of Dy nuclear spins in ferromagnetic Dy metal was found to be proportional to absolute temperature as described in the previous section. The nuclear spin-lattice relaxation in which the nuclear energy relaxes to the kinetic energy of a conduction electron is usually proportional to T. There are several interactions by which this type of relaxation is produced: Direct interactions of this kind are Fermi contact, dipole-dipole, orbital current and electric quadrupole interactions. The relaxation arised from these interactions have been calculated theoretically by Obata,[21] Yafet and Jaccarino,[22] and Moriya.[23] However, the relaxation due to these interactions is not important in ferromagnetic rare earth metals as will be discussed in next section.

An important contribution of the conduction electrons to the relaxation in heavy rare earth metals arises from the second order process in which the nuclear spin energy relaxes to the kinetic energy of conduction electrons via spin waves through the hyperfine interactions of 4f electrons and the sf exchange interactions. This is the extension of the relaxation mechanism proposed by Weger for 3d ferromagnetic metals[13] and will be discussed fully in IV, 2.

Linear temperature dependence of the relaxation rate can be obtained also by some other mechanisms. One of them is a direct process in which a spin wave is absorbed or emmitted when a nuclear spin flips. Because of energy conservation, only the spin wave whose frequency is equal to the NMR frequency can take part in this process. But the spin wave spectrum in ferromagnetic Dy metal has much larger energy gap than the NMR energy. Therefore, this direct process cannot occur. Another relaxation process of this kind is a direct process due to mixed mode of spin waves and elastic waves. Though this magneto-elastic interaction contributes little to the relaxation of Dy nuclei, a brief discussion will be given in the next section.

IV 2. The relaxation rate through hyperfine interactions of 4f electrons and sf exchange interactions via spin waves.

In ferromagnetic Dy metal, total angular momentum J of each magnetic ion couples together through strong exchange interactions. When a transition between nuclear spin levels takes place, a virtual spin wave can be excited by the hyperfine interaction between J and I. This virtual spin wave can be annihilated in a scattering process of the conduction electron through sf exchange interactions, transfering the nuclear energy to the change of the kinetic energy of conduction electron. The reverse process is also effective. This is the process to be considered in this sub-section. Weger[13] discussed the relaxation probability arising from this mechanism, in the case of magnetic hyperfine interaction and spherical Fermi surface. In the case of Dy metal, there exists a large electric

quadrupole hyperfine interaction beside magnetic one and also the Fermi surface of the conduction electrons is quite different from sphere as was shown by theoretical calculations of Keeton and Loucks.[24] Therefore an extension of Weger's calculation is needed.

When the total spin plus orbital angular momentum of each constitutional ion of a magnetic system is a good quantum number, the magnetic and electic quadrupole hyperfine Hamiltonian of the j-th nucleus can be written in the form

$$\mathcal{H}_{hyp.} = A\mathbf{J}_j \cdot \mathbf{I}_j - B\Big[\frac{1}{3}\{3J_{jz}^2 - J(J+1)\}\{3I_{jz}^2 - I(I+1)\} + \frac{1}{2}\{(J_{jz}J_{j+} + J_{j+}J_{jz}) \times (I_{jz}I_{j-} + I_{j-}I_{jz}) + (J_{jz}J_{j-} + J_{j-}J_{jz})(I_{jz}I_{j+} + I_{j+}I_{jz})\} + \frac{1}{2}(J_{j+}^2 I_{j-}^2 + J_{j-}^2 I_{j+}^2)\Big]. \tag{4, 1}$$

Here, $\mathbf{J}_j$ is the total angular momentum of the j-th ion at the lattice site $\mathbf{R}_j$, $\mathbf{I}_j$ the nuclear spin of the j-th nucleus and the z-axis is along the easy direction of magnetization. $J_{\pm}$ are $J_x \pm J_y$ and $I_{\pm}$ are $I_x \pm I_y$ respectively and A and B are given by

$$\left.\begin{aligned} A &= 2\beta(\mu_I/I)\langle r^{-3}\rangle\langle J\|N\|J\rangle(1-R_m) \\ B &= \frac{3e^2Q}{4I(2I-1)}\langle J\|\alpha\|J\rangle\langle r^{-3}\rangle(1-R_Q). \end{aligned}\right\} \tag{4, 2}$$

where $\langle J \| N \| J\rangle$ and $\langle J \| \alpha \| J\rangle$ are pure numbers which are tabulated in the paper of Elliott and Stevens[25] for the ground state of 4f ions. μ_I is the magnetic moment of the nucleus, β the Bohr magneton, Q the nuclear electric quadrupole moment, $\langle r^{-3}\rangle$ the average of r^{-3} of 4f electron and R_m and R_Q are the shielding factors of the closed shell electrons.

It is convenient to transform the hyperfine interaction Hamiltonian using the transformation of Holstein and Primakoff;[26]

$$J_{jz} = J - a_j^* a_j, \quad J_{j+} = (2J)^{\frac{1}{2}} a_j, \text{ and } J_{j-} = (2J)^{\frac{1}{2}} a_j^*. \tag{4, 3}$$

In these expressions, a_j^* and a_j are Bose creation and annihilation operators, respectively. Since the number of excited spin waves is generally small at low temperature, the factor $(1-a_j^* a_j/2J)$ is already approximated to be unity.

We keep terms only to the first order in $I_\pm$, a^* and a, because the contribution of the second order terms to the relaxation is smaller in the order of magnitude. A brief comment of the relaxation rate due to higher order terms in $I_\pm$ and $J_\pm$ will be given later. The retained terms in the hyperfine interaction can be written as $\mathcal{H}^{\circ}_{hyp.} + \mathcal{H}'_{hyp.}$ which are given approximately by

$$\mathcal{H}^{\circ}_{hyp.} = AJ I_{j z} - \frac{2}{3} BJ^2 [3 I_{j z}^2 - I(I+1)] \qquad (4, 4)$$

$$\mathcal{H}'_{hyp.} = \frac{A}{2}(2J)^{1/2}(a_j I_{j-} + a_j^* I_{j+}) - B(2J)^{1/2} J [I_{j z}(a_j I_{j-} + a_j^* I_{j+}) + (a_j I_{j-} + a_j^* I_{j+}) I_{j z}]. \qquad (4, 5)$$

Here, because of large value of J, (1-1/2J) is approximated to be unity.

Further, we transform a_j^* and a_j to their Fourier transforms a_q^* and a_q;

$$a_j = N^{-\frac{1}{2}} \sum_q e^{-iqR_j} a_q \quad \text{and} \quad a_j^* = N^{-\frac{1}{2}} \sum_q e^{iqR_j} a_q^*, \qquad (4, 6)$$

where N is the total number of atoms in the crystal. Then the hyperfine Hamiltonian $\mathcal{H}'_{hyp.}$ which gives the relaxation is transformed as follows

$$\mathcal{H}'_{hyp.} = \left(\frac{A}{2}\right)(2J)^{\frac{1}{2}} N^{-\frac{1}{2}} \left[\sum_q e^{-iqR_j} a_q I_{j-} + \sum_q e^{iqR_j} a_q^* I_{j+}\right] - B(2J)^{\frac{1}{2}} N^{-\frac{1}{2}} J \left[I_{j z}\left(\sum_q e^{-iqR_j} a_q I_{j-} + \sum_q e^{iqR_j} a_q^* I_{j+}\right) + \left(\sum_q a^{-iqR_j} a_q I_{j-} + \sum_q e^{iqR_j} a_q^* I_{j+}\right) I_{j z}\right] \qquad (4, 7)$$

On the other hand, denoting the annihilation and creation operators for the conduction electrons having the wave vectors k and k' and the spin up and down as $b_{k\uparrow}$ and $b_{k'\downarrow}$, respectively, the part of the sf exchange Hamiltonian which relates to the relaxation can be written as

$$\mathcal{H}'_{sf} = -N^{-1}\sum_{k,k'}\sum_{n}(g_J-1)\mathcal{J}(k,k')e^{i(k-k')R_n}(b^*_{k'\downarrow}b_{k\uparrow}J_{n+}+b^*_{k'\uparrow}b_{k\downarrow}J_{n-}). \quad (4,\ 8)$$

Here, g_J is the Landé factor and $\mathcal{J}(kk')$ is given by

$$\mathcal{J}(k,k') = \int e^{i(k-k')r}u^*_{k'}(r)\,u_k(r)\,\mathcal{J}(r)\,dr \quad (4,\ 9)$$

where $u_k(r)e^{ikr}$ is the Bloch function of the band electron and $\mathcal{J}(r)$ is the exchange interaction function between the band electron and the 4f electron. Next, $\mathcal{H}'_{sf}$ is transformed to be represented by a^*_q and a_q instead of $J_\pm$. The result is

$$\mathcal{H}'_{sf} = -N^{-1}N^{-\frac{1}{2}}(2J)^{\frac{1}{2}}\sum_{k}\sum_{n}(g_J-1)\mathcal{J}(kk')e^{i(k-k')R_n} \quad (4,\ 10)$$
$$\times\{b^*_{k'\uparrow}b_{k\downarrow}\sum_q e^{iqR_n}a^*_q + b^*_{k'\downarrow}b_{k\uparrow}\sum_q e^{-iqR_n}a_q\}.$$

By the Hamiltonian $\mathcal{H}'_{hyp.}$ only the transitions between the nuclear levels $\Delta m=\pm 1$ are allowed as only one magnon process is concerned. Because the transition probability $m\to m+1$ is equal to $m+1\to m$, we calculate only the probability of the transition $m\to m+1$. The matrix element of $\mathcal{H}'_{hyp.}$ in which the spin state of the j-th nucleus changes from m to m+1 and at the same time a spin wave of the wave number q is excited is given by

$$\langle m+1, q|\mathcal{H}'_{hyp.}|m, 0\rangle = \sqrt{(I-m)(I+m+1)}(2J)^{\frac{1}{2}}N^{-\frac{1}{2}}\sum_q e^{iqR_j}\left[\frac{A}{2}-BJ(2m+1)\right]. \quad (4,11)$$

The energy difference between m and m+1 levels, $\hbar\omega_{m,m+1}$, is given by

$$\hbar\omega_{m,m+1} = AJ - 2BJ^2(2m+1) \quad (4,\ 12)$$

Therefore

$$\langle m+1, q|\mathcal{H}'_{hyp.}|m, 0\rangle = \sqrt{(I-m)(I+m+1)}\,(2J)^{-\frac{1}{2}}N^{-\frac{1}{2}}(\hbar\omega_{m,m+1})\sum_q e^{iqR_j}.$$

On the other hand, the matrix element in which a conduction electron $k\uparrow$ is scattered by an ion to the state $k'\downarrow$ absorbing a spin wave of the wave number q is given by $\langle k'\downarrow, 0|\mathcal{H}'_{sf}|k\uparrow, q\rangle$ which is calculated from (4, 10) as

$$\langle k'\downarrow, 0|\mathcal{H}'_{sf}|k\uparrow, q\rangle = -N^{-1}N^{-\frac{1}{2}}(2J)^{\frac{1}{2}}(g_J-1)\sum_n \mathcal{J}(k,k')e^{i(k-k')R_n}e^{-iqR_n}. \quad (4,\ 13)$$

Thus, the second order perturbation matrix element corresponding to the transition from the state of the nucleus m and the state of conduction electron $k\uparrow$ to m+1 and $k'\downarrow$ is given by

$$\langle k'\downarrow, m+1 | \mathcal{H}'_{hyp.} | s_j | k\uparrow, m \rangle = -N^{-2}\sqrt{(I-m)(I+m+1)}\,(\hbar\omega_{m,m+1})\,\mathcal{J}(k,k') \times (g_J-1)\sum_{q} e^{iqR_j}\sum_{n} e^{i(k-k'-q)R_n} \Big/ [E(q)+\mathcal{E}(m+1)-\mathcal{E}(m)] \quad (4,14)$$

where E(q) is the energy of the spin wave having the wave vector q and $\mathcal{E}(m)$ and $\mathcal{E}(m+1)$ are the energies of the nuclear states m and m+1, respectively. Because the energy of the spin wave is very much larger than the energy difference of the nuclear levels, $\mathcal{E}(m+1)-\mathcal{E}(m)$ in the denominator can be neglected. Now

$$\sum_{n} e^{i(k-k'-q)R_n} = N \quad (4,15)$$

only when $k-k'-q=G_i$, where G_i is one of the reciprocal lattice vectors, and otherwise it is zero. Here, k and k' are taken in the first zone. The case in which $G_i=0$ corresponds to the normal process, and the case in which G_i is non-zero corresponds to the umklapp process. Taking these considerations into account, the matrix element is transformed to

$$\langle k'\downarrow, m+1 | \mathcal{H}'_{hyp.} | s_j | k\uparrow, m \rangle = -N^{-1}\sqrt{(I-m)(I+m+1)}\,(\hbar\omega_{m,m+1}) \times (g_J-1)\,\mathcal{J}(k,k')\sum_{i}\frac{e^{i(k-k'-G_i)R_j}}{E(k-k'-G_i)} \quad (4,16)$$

where the sum is over all possible reciprocal lattice vectors.

From this matrix element, the transition probability from the nuclear state m to m+1 by this process is calculated to be

$$W_{m,m+1} = \left(\frac{2\pi}{\hbar}\right)\sum_{k,\,occup.}\sum_{k',\,unoccup.}\left(\frac{(g_J-1)}{N}\mathcal{J}(k,k')\right)^2(\hbar\omega_{m,m+1})^2 \times [(I-m)(I+m+1)]\left|\sum_{i}\frac{e^{i(k-k'-G_i)R_j}}{E(k-k'-G_i)}\right|^2 \delta(E_i-E_f). \quad (4,17)$$

Here the last factor, $\delta(E_i-E_f)$, is the energy conservation term between the initial and final states and the summations

in k and k' extend over all occupied and unoccupied states, respectively. In this expression,

$$\left| \sum_i \frac{e^{i(k-k'-G_i)R_j}}{E(k-k'-G_i)} \right|^2 = \sum_{i,l} \frac{e^{i(G_i-G_l)R_j}}{E(k-k'-G_i)E(k-k'-G_l)} \qquad (4, 18)$$

and since $G_i - G_l$ is also one of the reciprocal lattice vectors, $\exp\left[i(G_i-G_l)R_j\right]$ is equal to unity. Then, transforming summations in k and k' into integrals, and neglecting the nuolear energy in $E_i - E_f$, we obtain

$$W_{m,m+1} = \left(\frac{2\pi}{\hbar}\right)(\hbar\omega_{m,m+1})^2[(I-m)(I+m+1)]\int dk \int dk' [(g_J-1)\mathcal{J}(k,k')]^2$$

$$\times \sum_{i,l} \frac{1}{E(k-k'-G_i)E(k-k'-G_l)} f(E_{k\uparrow})[1-f(E_{k'\downarrow})]\delta(E_{k\uparrow}-E_{k'\downarrow})\eta(k\uparrow)\eta(k'\downarrow), \qquad (4, 19)$$

where $f(E_{k\uparrow})$ and $f(E_{k'\downarrow})$ are the Fermi functions of up and down spin electrons and $\eta(k\uparrow)$ and $\eta(k'\downarrow)$ are the densities of states for these electrons.

Because of the Fermi factors, the integration is restricted on the Fermi surfaces of the up and down spin electrons, and the final result of the transition probability is given by

$$W_{m,m+1} = \left(\frac{2\pi}{\hbar}\right)(\hbar\omega_{m,m+1})^2(I-m)(I+m+1)k_B T \int d\sigma_k \int d\sigma_{k'}$$

$$\times \sum_{i,l} \frac{1}{E(k-k'-G_i)E(k-k'-G_l)} g(k\uparrow)g(k'\downarrow)(g_J-1)^2[\mathcal{J}(k,k')]^2, \qquad (4, 20)$$

where k_B is the Boltzmann factor, T the absolute temperature, $g(k\uparrow)$ and $g(k'\downarrow)$ the densities of states of the conduction electrons of $k\uparrow$ and $k'\downarrow$ per atom and per unit energy on the corresponding Fermi surfaces and $d\sigma_k$ and $d\sigma_{k'}$ are the surface element on the corresponding Fermi surfaces at the values k and k', respectively.

In this expression, the local density of states $g(k\uparrow)$ or $g(k'\downarrow)$ and the functional form of $\mathcal{J}(kk')$ are not known. Therefore, for a numerical estimation of the transition probability, we have to make some approximations; we replace

$\mathcal{J}(kk')$ by a constant value $\mathcal{J}$ which corresponds to some appropriate average of $\mathcal{J}(kk')$ over k and k' in the first zone and also we replace $g(k\uparrow)$ and $g(k'\downarrow)$ by an average value $N(E_F)/A$ where $N(E_F)$ is the density of states per unit energy all over the Fermi surface for electron having one direction of spin and A is the total area of the Fermi surface. Here the difference of the Fermi surfaces of up and down spin electrons is neglected. Then the transition probability is given by

$$W_{m,m+1} = \left(\frac{2\pi}{\hbar}\right)(\hbar\omega_{m,m+1})^2 (I-m)(I+m+1) k_B T \left(\frac{N(E_F)}{A}\right)^2 \mathcal{J}^2 (g_J-1)^2 \times \int d\sigma_k \int d\sigma_{k'} \sum_{i,l} \frac{1}{E(k-k'-G_i)\, E(k-k'-G_l)} . \qquad (4, 21)$$

Numerical calculation of $W_{m,m+1}$ by the use of the theoretical Fermi surface and spin wave spectrum will be given in next section.

$W_{m,m+1}$ given by (4, 20) or (4, 21) is proportional to T and $\omega^2_{m,m+1}$, in accordance with the conclusion obtained from the analysis of the experimental relaxation curves.

In Weger's original calculation,[13] only the magnetic hyperfine interaction is taken into account and by assuming that the Fermi surface does not approach the zone boundaries, the umklapp processes are neglected. Contrary to the case of 3d metals, the shape of the Fermi surface of rare earth metals is quite anisotropic and the Fermi surface touches the zone boundaries, so that the umklapp processes may have an important contribution. Moreover, the cross terms of the normal and umklapp processes should be taken into accoount. Further discussions will be given in next section.

In the above calculation, the last term in (4, 1) which gives the transitions $\Delta m = \pm 2$ by the nuclear electric quadrupole

interaction is neglected. This term contains a^2 and a^{*2}, and for the calculation of the transition probability corresponding to $\Delta m=\pm 2$, the processes containing two magnon excitation should be taken into account. The transition probability by this process can be calculated by a third order perturbation calculation in a similar way to that described above. It is easily shown that this probability is very much smaller than that given by (4, 21) and moreover it is proportional to the cube of T. Thus the transitions $\Delta m=\pm 2$ have negligible contributions to the relaxation in our case.

IV 3. The spin-spin relaxation

Here we shall give a brief discussion on the Walstedt's mechanism[14] in ferromagnetic Dy metal.

When a 90° pulse is applied to observe the echo of NMR at the frequency $\omega_{m,m+1}$, a transverse magnetization is produced which rotates in a plane perpendicular to the internal field with the frequency $\omega_{m,m+1}$. The intensity of the echo signal is proportional to n_+-n_-, where n_+ and n_- are the populations in the states of nuclear magnetization parallel and antiparallel, respectively, to the quantization axis in the plane perpendicular to the internal field in the rotating coordinate system, rotating with the frequency $\omega_{m,m+1}$ relative to the laboratory system. The axis of quantization for other m' states than m and m+1 are taken in the direction of the internal field and the population in the m' state is denoted as $n_{m'}$. Then Walstedt shows that the differential equation for the decay of n_+-n_- can be given by

$$\frac{d(n_+ - n_-)}{dt} = -(W_{+-} + W_{-+})(n_+ - n_-) - n_+ \sum_{m'} W_{+,m'} + n_- \sum_{m'} W_{-,m'} + \sum_{m'} n_{m'} W_{+,m'} - \sum_{m'} n_{m'} W_{-,m'} \qquad (4, 22)$$

where $W_{i,j}$ is the relaxation probability between the states i and j.

If we take only the relaxation given in IV, 2 into account, $W_{i,j}$ in this expression can be expressed by $W_{m,m+1}$ as follows;

$$\left.\begin{aligned} W_{+-} &= W_{-+} = W_{m,m+1}/2 \ * \\ W_{+,m+2} &= W_{-,m+2} = W_{m+1,m+2}/2 \\ W_{+,m-1} &= W_{-,m-1} = W_{m-1,m}/2 \\ W_{+,m'} &= W_{-,m'} = 0, \text{ for } m' \text{ other than } m+2 \text{ and } m-1. \end{aligned}\right\} \qquad (4, 23)$$

Then the differential equation becomes very simple;

$$\frac{d(n_+ - n_-)}{dt} = -\left(W_{m,m+1} + \tfrac{1}{2} W_{m-1,m} + \tfrac{1}{2} W_{m+1,m+2}\right)(n_+ - n_-). \qquad (4, 24)$$

Thus the echo decay is given by a simple exponential function, $\exp(-t/T_2)$, where T_2 is given by

$$1/T_2 = W_{m+1,m+2}/2 + W_{m,m+1} + W_{m-1,m}/2 \qquad (4, 25)$$

In the case of the highest or lowest frequency line, either one of the first or third term in the right hand side of this equation is, of course, zero. The relaxation time given in (4, 25) will be compared with the experimental value in next section.

---

* In the original expression of Walstedt, the contribution from the interaction term containing I_z is treated as equally effective as those containing I_x and I_y, and a slightly different expression is given for W_{+-} or W_{-+}. In the relaxation process discussed in IV, 2, there is no contribution

from a term containing I_z to the relaxation, and this simple relation holds.

V. Discussions

V 1. The spin-lattice relaxation.

Before entering the discussion of the relaxation due to the peocess disoussed in IV, 2 which is the main term in Dy metal, we first consider briefly the relaxation arising from direct interactions with the conduction electrons. The most important one is the Korringa mechanism.[19] The transition probability $W^{(K)}_{m,m+1}$ between the nuclear levels m and m+1 by the Fermi contact interactions of the conduction electrons is given by

$$W^{(K)}_{m,m+1} = a_0 \left| (m \left| I_+ \right| m+1) \right|^2$$

$$a_0 = \frac{64}{9}\pi^3 \hbar^3 \gamma_e^2 \gamma_n^2 \left(\left| \psi_{E_F}(0) \right|^2 \right)^2 k_B T [N(E_F)]^2 \qquad (5, 1)$$

where γ_e and γ_n are the gyromagnetic ratios of electron and nucleus, respectively, $\left|\psi_{E_F}(0)\right|^2$ the density of the conduction electron on the Fermi surface at the nuclear site, and $N(E_F)$, the density of states on the Fermi surface.

From Mössbauer isomer shift, Herring et al.[27] obtained the value of $|\psi(0)|^2$ which is the density per atom of a conduction electron at the nuclear site. Here $|\psi(0)|^2$ is the average value over whole conduction electrons, contrary to the case of $|\psi_{E_F}(0)|^2$ in which only the electrons on the Fermi surface are considered. Their result is $|\psi(0)|^2 = (1.65 \pm 0.35) \times 10^{-26} \mathrm{cm}^{-3}$. If we assume that the density at the nucleus of the electrons on the Fermi surface is the same as this, the value a_0 can be numerically computed. Using the value of $N(E_F)$ given in Table 2, which is the value obtained by the theoretical calculation of Keeton and Loucks,[24] we obtain about 10^2 T for a_0, and W_0 or $W_{3/2,-5/2}/T$

defined in III becomes about 5×10^{2} $sec^{-1}{}^{\circ}K^{-1}$, which is about the same magnitude as the experimental value. However, $W^{(K)}_{m,m+1}$ is independent of $\omega_{m,m+1}$ and the decay curves expected from this process follow the curves given in Fig.7 (case 1 in Appendix) which are entirely in disagreement with the experimental curves. Then why doesn't the Korringa mechanism take part in the relaxation of Dy spins? Probably this arises from the fact that the conduction electrons on the Fermi surface are mostly in non-s states and the value of $|\psi_{E_F}(0)|^2$ is much smaller than $|\psi(0)|^2$ which is the average density for whole electrons at the nuclear site. This means that the conduction electrons having s-character mostly have smaller energies than the Fermi energy and sink in the low energy part in the band.

This consideration holds also in the numerical estimate of the magnetic hyperfine field. If we assume that $|\psi_{E_F}(0)|^2$ were equal to $|\psi(0)|^2$ given by Mössbauer experiment and if we assume a uniform polarization model for the conduction electrons, the internal field at the nucleus would be calculated using the value of the sf exchange interaction energy which is given in Table 2 to be about -4500 Koe which is about the same as the field produced by 4f electrons. However, because the hyperfine field in rare earth metal is accounted for mainly by that of 4f electrons, the contribution from the polarization of the conduction electrons should be much smaller than the value given here. In this case too the smallness of s-character for the electrons on the Fermi surface is probably the origin of this reduction of the hyperfine field. Taking the value -270 Koe for the hyperfine field due to the conduction electron

polarization, which was given in III, the fraction of s-character in the electronic states at the Fermi surface is estimated to be about 1/15.

Narath in his discussion on the Knight shift and spin-lattice relaxation in hexagonal La metal[28] which probably has a similar Fermi surface as Dy metal, also showed the smallness of the s-character for the electrons at the Fermi surface. Rough estimate shows that the reduction of the s-character of the electrons at the Fermi surface to about 1/15 gives right order of magnitudes for the Knight shift and spin-lattice relaxation time for La metal.

Considering from these facts, the smallness of the s-character of the electrons at the Fermi surface is not a special property in Dy metal but is a general property in metals in which the Fermi surface is given by similar shape, such as Y, La and other heavy rare earth metals. All in these metals, the shape of the Fermi surface is quite different from that expected by free electron model, but has nearly the same anisotropy.

If we assume that $|\Psi_{E_F}(0)|^2$ is about 1/15 of $|\Psi(0)|^2$, the calculated Korringa relaxation probabilities are two or more orders of magnitude smaller than the observed ones and are entirely negligible.

The spin-lattice relaxation arising from other hyperfine interactions of the conduction electrons than Fermi contact one is also estimated for Dy metal. Among various interactions, the nuclear quadrupole interaction takes a most important part. But the estimated value of the relaxation probability is very much smaller than the observed value and is quite negligible.

Next, the relaxation by the Weger's process given in IV, 2 will be discussed. For the numerical estimate of $W_{m,m+1}$ given in (4, 21), values of various quantities contained in the equation should be known. We first discuss these. A number of authors have discussed the spin wave spectrum of ferromagnetic Dy metal. Cooper[29] calculated theoretically the spectra at absolute zero temperature which are shown in Fig.5 a and b. An interesting feature is a flat portion for small q region in the c-direction. Direct observation of the spin wave spectrum has been made in ferromagnetic Tb metal[30] by neutron scattering technique. Because detailed shape of the spectrum does not affect the final result of our rough numerical estimation of $W_{m,m+1}$, we approximate the spin wave spectrum to be represented by

$$E(q) = \hbar\omega(q) = \Delta(q_c) + D(q_a^2 + q_b^2) \qquad (5, 2)$$

where $\omega(q)$ is the frequency of the spin wave having the wave vector q and the a-, b- and c-axes are taken in the directions of the crystallographic axes of the hexagonal lattice. $\Delta(q_c)$ is assumed to follow the curve shown in Fig.5, a, but for numerical calculation of $W_{m,m+1}$ this curve is further approximated by a step function shown by dotted line in this figure. Though the curve shown in Fig.5, b is not a quadratic function, we approximate it to be a quadratic one, and the constant D in (5, 2) is determined from the spin wave energies at $q_a=0$ and $q_a=\pi/a$ in Fig.5, b.

To calculated $W_{m,m+1}$, the shape of the Fermi surface should be known. The band calculation of Keeton and Loucks[24] shows that the shape of the Fermi surface of Dy metal in paramagnetic phase is quite complicated and it is almost impossible

to do the integration in (4, 21) over this Fermi surface. Therefore, retaining typical features of the calculated Fermi surface, we approximate the surface to that shown in Fig.6. There are a hole surface and an electron surface in reduced zone representation.

Though the local density of states is not given, Keeton and Loucks calculated the density of state of the conduction electons at the Fermi surface per atom and per unit energy. The density of states calculated from the observed electronic specific heat[31] is about twice as large as this theoretical value. However, because the effect of electron-phonon interaction is not known accurately, we use the value of Keeton and Loucks in numerical calculation of $W_{m,m+1}$ by (4,21). Further, the Fermi surfaces for up and down spin electrons in ferromagnetic phase may differ appreciably from that in paramagnetic phase. However because of lack of the calculation in ferromagnetic phase, we have to use the paramagnetic Fermi surface for both up and down spin electrons in ferromagnetic phase.

Next a brief discussion will be given on $\mathcal{J}$. Assuming an uniform polarization model for the conduction electrons, Jaccarino et al.[32] obtained the value of $\mathcal{J}$ from the Knight shift of Al in XAl_2 alloys in which X is either one of rare earth metals, In the definition given in IV, 2, the sf exchange energy is expressed as $-2\mathcal{J}$ sS or $-2\mathcal{J}$ (g_J-1)sJ where s is the spin of the conduction electron and S is the spin angular momentum of unfilled 4f shell. The value obtained by them is $2\mathcal{J} \cong -0.1$ eV. Later, Barnes and Jones[33] repeated similar experiments, but they found that the Knight shift in non-magnetic rare earth di-aluminide which has to be used in the calculation of $\mathcal{J}$ as a standard of Knight shift,

was different from that used by Jaccarino et al., The revised value of $2\mathcal{J}$ using their new value of the standard Knight shift is $2\mathcal{J} = -0.3$ eV. On the other hand, from the value of the hyperfine field of the conduction electrons in Dy metal, -270 Koe, given in III and from the Knight shift in paramagnetic La metal obtained by Narath,[28] 0.83% (average value for two different sites), the value of $\mathcal{J}$ can be estimated. Assuming that the values of $|\Psi_{E_F}(0)|^2$ and the density of states of the conduction electrons at the Fermi surface in La metal are respectively the same as those in Dy metal, which may be plausible assumption in our approximate calculation, $2\mathcal{J}$ is estimated to be about -0.1 eV. Because of various ambiguities in determining the value of $\mathcal{J}$ from these experiments, it is hopeless to know accurate value, but all these experiments give $2\mathcal{J}$-values of a few tenth of eV. Therefore for the calculaton of $W_{m,m+1}$, we assume $2\mathcal{J} = -0.15$ eV as an approximate value.

Another method of determining $\mathcal{J}$ is to use the magnetization per atom in ferromagnetic phase. The main contribution to the magnetization arises from 4f electrons, but some minor contribution arises from the polarization of the conduction electrons induced by sf exchange interactions. This contribution is obtained by subtracting the calculated 4f contribution from the experimental magnetization per atom. By this consideration, $2\mathcal{J}$ value of about +0.1 eV was obtained.[34] Though the absolute value of $2\mathcal{J}$ estimated from the Knight shift or internal field agrees well with that estimated from the magnetization, the sign is different. So, there remains a serious ambiguity in determining $\mathcal{J}$ from these experiments. In the equation of $W_{m,m+1}$, $\mathcal{J}$ enters in a quadratic form and its sign does not affect the

final result. The same holds for the calculation of the exchange interaction between localized magnetic moments in heavy rare earth metals.

Knowing values of various quantities appeared in (4, 21), numerical estimation of $W_{m,m+1}$ was performed. In the integration over the Fermi surface, further mathematical approximations was made for simplicity which does not affect much the final result. The values of various parameters used in the calculation together with the result are shown in Table II. The calculated value of W_o is $\sim 4 \times 10^2$ $sec^{-1} {}^\circ K^{-1}$ and is quite in good agreement with the experimental value, 4.76×10^2. An important feature in the result of the calculation is that the normal process, the umklapp processes and their mixed terms contribute to the relaxation with about the same weights. Because of the uncertainties in various parameters, and rough approximations made in the calculation, the computed value is only a tentative one, but it seems certain that the Weger's process, that is, the relaxation process via spin waves through 4f hyperfine interactions and sf exchange interactions is the main one for the nuclear spin-lattice relaxation in ferromagnetic Dy metal.

A similar calculation was also made by assuming a free-electron-like spherical Fermi surface of radius 1.4×10^8 cm^{-1} which is given by $(3\pi^2 N_e)^{1/3}$, N_e being the number of electrons per cc. With the values of $N(E_F)$ and γ shown in Table II, the calculated value of W_o is about 1/50 of that calculated above by the use of the Fermi surface shown in Fig.6, and this value of W_o is in quite disagreement with the experimental value. Therefore it seems that the non-spherical shape of the conduction electron Fermi surface is important to give a right value for

W_o. In the case of spherical Fermi surface, only the normal process is important.

One more possible relaxation mechanism which arises from magneto-elastic coupling will be discussed next, though it will be shown finally that its contribution to the relaxation is negligible. It is a process similar to that proposed by Pincus and Winter.[35] Suppose that the lattice is deformed periodically by an elastic shear wave of long wave length, which is excited thermally. It seems probable that in this case the total angular momentum J of each ion also makes an torsional vibration about its equilibrium direction with the same frequency as that of the elastic wave. The amplitude of the torsional vibration is determined by the magneto-elastic coupling, being proportional to the amplitude of the shear wave. Through the hyperfine coupling between J and I, an oscillating magnetic field as well as an oscillating electric field gradient will be produced at each nucleus, which produce the relaxation of the nuclear spin, if the frequency of the shear wave coincides with the frequency of a possible nuclear transition. Because the anisotropy energy in the plane containing the c-axis is about two order of magnitude larger than that in the c-plane in ferromagnetic Dy metal, only the shear wave in the c-plane is effective to the relaxation. The relaxation probability by this mechanism can be calculated following standard method of calculating spin-lattice relaxation and the result is given by

$$W_{m,m+1}^{(me)} = \frac{\omega_{m,m+1}^4 (\tilde{\beta}\gamma)^2 J^2}{12\pi^2 \rho (\delta_e \hbar H_{anis.}^2) v_{elas.}^5} [I(I+1)-m(m+1)] k_B T, \qquad (5, 3)$$

where ρ is the density of crystal, $H_{anis.}$ is the planer hexagonal

anisotropy field, v_{elas} is the velocity of shear wave in the c-plane and $\tilde{B}^{\gamma}$ is the magneto-elastic coupling constant as defined by Callen and Callen.[36] $W^{(me)}_{m,m+1}$ is numerically computed by the use of following values for constants appeared in (5, 3):

$$\rho = 8.536\ \mathrm{gr\cdot cm^{-3}},\quad v_{elas.} = 1.72\times10^{5}\ \mathrm{cm\cdot sec^{-1}}\ [37],\quad \gamma_{eff} H_{ani.} = 3.3\times10^{-16}\ \mathrm{erg\cdot atom^{-1}}\ [38],$$
$$\tilde{B}^{\gamma} = 7.43\times10^{-15}\ \mathrm{erg\cdot atom^{-1}}\ [39].$$

The result is $W^{(me)}_{o} = 2\times10^{-3}$ and is many orders of magnitude smaller than the experimental value. Thus the contribution of this process to the relaxation is quite negligible. $W^{(me)}_{m,m+1}$ is proportional to $\omega^{4}_{m,m+1}$, and if this process were dominant, the relaxation decay would follow the curves shown in Fig.9.

From these considerations, it may be concluded that the importance of the Weger's mechanism in the nuclear spin-lattice relaxation may be generally true not only for Dy metal but also for all ferromagnetic non-S heavy rare earth metals.

V 2. The spin-spin relaxation time.

In IV, 3, we calculated the contribution of the spin-lattice relaxation to T_2, the transverse relaxation time or the time constant of the decay of the echo envelope. Using the value of W_o ($= 4.76\times10^{2}$) obtained from the experiments of the spin-lattice decay, we calculated the value of $1/T_2$ for the transition $1/2 \leftrightarrow -1/2$ of Dy^{163} by the equation (4, 25). The result is $1/T_2 T = 1.94\times10^{4}\ \mathrm{sec^{-1}}$. This relation is shown by a solid line in Fig.4. The agreement between this line and the experimental plots is satisfactory, indicating that the spin-spin relaxation in Dy metal is determined solely by the spin-lattice relaxation. Because $W_{m,m+1}$ is proportional to $\omega^{2}_{m,m+1}$, the shorter T_2 is the larger $\omega_{m,m+1}$ is. This also agrees with the experimental

results.

Now, in ferromagnetic material, an important spin-spin relaxation arises from Suhl-Nakamura interaction,[20] the I-I coupling produced by the second order process of the hyperfine interactions via spin waves. Sherrington[40] have calculated the transverse relaxation time in ferromagnetic Dy metal due to this mechanism. The calculated value is approximately 6 microsecond. This value is smaller than the experimental value. Because T_2 due to this mechanism is expected to be independent of temperature in (liquid) helium temperature range, it must be the case that the Suhl-Nakamura interaction is made ineffective by some reasons in actual Dy metal.

The inefficiency of the Suhl-Nakamura interaction to the spin-spin relaxation in Dy metal probably arises from the inhomogeneity in the broadening of NMR lines. As already described in III, each line has a width of several MHz, which is much larger than the width expected from T_2. Only a hot spot at the frequency of the applied rf field contributes to the resonance. Therefore, spin-spin relaxation due to I·I coupling is effective only for the nuclei having the same frequency as that of the hot spot. Because the frequency width of the hot spot is a fraction of MHz (a rf pulse of about one microsecond width corresponds to 90° pulse in our experimental condition), only about a few per cent of the nuclei contributing to the whole line width are effective to T_2 through I·I couplings. This situation is similar to the case of diluted crystal and the spin-spin relaxation time due to I·I coupling will become several ten times longer than that calculated for the homogeneous line.[41] Considering from the proportionality of $1/T_2$ to T, the spectral diffusion

time too seems to be much longer than the observed T_2. both the spin and spectral diffusions contribute little to the spin-spin decay of the hot spot. Experiment at still low temperature or by more perfect crystal should be needed to observe the effect of I I coupling on the spin-spin relaxation.

Acknowlegements

The author would like to express his gratitude for the continuous guidance and encouragement of Professor J. Itoh, under whose direction this work was performed. He is much indepted to Dr. S. Kobayashi for the stimulation and guidance in initiating this work. He also wish to thank Professors T. Moriya, T. Nakamura, and K. Yoshida for their valuable discussion on the spin-lattice relaxation and to Professor K. Asayama for valuable discussion.

Appendix. The solution of rate equations for the spin-lattice relaxation.

Functional forms of the spin-lattice relaxation decay in the case of I=5/2 are calculated under the assumption that the nuclear energy levels are unequally spaced and the transition probability depends upon the spacing of the nuclear levels.

Let $N_m(t)$ be the population of the m-th level at a time t and N_m° be the thermal equilibrium population of the m-th level. A family of rate equations of the spin-lattice relaxation is written as

$$dn_m/dt = \sum_m W_{m,n}(n_n - n_m) \qquad \text{(A, 1)}$$

where $n_m=(N_m(t)-N_m^\circ) / \sum_m N_m^\circ$ and is the relative deviation of the pupulation of the m-th level from the thermal equilibrium value, and $W_{m,n}$ is the spin-lattice relaxation probability

between the m-th and n-th levels. Defining a quantity a_m by $a_m = n_m - n_{m+1}$, which is proportional to the intensity of the stimulated echo for the transition between the levels m and m+1, 2I coupled linear differential equations for a_m are obtained from (A, 1);

$$da_m(t)/dt = \sum_k w_{m,k} a_k(t). \qquad (A, 2)$$

We assume that only the transitions $\Delta m = \pm 1$ are thermally allowed. Then $w_{m,k}$ is given by

$$w_{m,k} = W_{m-1,m}\delta_{m-1,k} - 2W_{m,m+1}\delta_{m,k} + W_{m+1,m+2}\delta_{m+1,k}. \qquad (A,3)$$

The solution of (A, 2) is expressed in the form

$$a_m(t) = \sum_j a_j^{(m)} \exp(-\lambda_j t) \qquad (A,4)$$

Here $a_j^{(m)}$'s are determined by the initial conditions, while λ_j's are determined by $W_{m,n}$, solving a secular equation.

Case 1.

When the relaxation probability $W_{m,m+1}$ is only proportional to $I(I+1)-m(m+1)$ which is $|(m|I_x|m+1)|^2$, being independent of $\omega_{m,m+1}$, Andrew and Turnstall[18] have obtained the general solution for λ_j;

$$\lambda_j/W = (j+I)(j+I+1) \qquad (A, 5)$$

where W is the proportionality constant of $W_{m,m+1}$ and j is either one of possible m values.

In the case when the relaxation decay of the NMR line corresponding to the transition between the m-th and (m+1)-th levels is measured by stimulated echo method, the initial conditions are given simply by $a_{m+1}(0)=a_{m-1}(0)=\beta$, $a_m(0)=-2\beta$ and $a_{m'}(0)=0$ for m' other than m-1, m and m+1, where $\beta=(h\omega_{m,m+1}/2k_BT)(N/6)$, N being the total number of nuclei. Full discussion of the results was already given by Andrew and Turnstall, and others[18], and only the calculated relative decay curves of

the stimulated echo signal are shown in Fig.7, for all resonance lines.

Case 2.

In the case when the transition probability $W_{m,m+1}$ is proportional to $[I(I+1)-m(m+1)]\cdot\omega^2_{m,m+1}$, the numerical solution of the secular equation for λ_j gives

$$\lambda_j/W_{-3/2,-5/2} = 1.06,\ 7.34,\ 23.11,\ 53.67 \text{ and } 105.00 \qquad (A,\ 6)$$

for j=1, 2, 3, 4 and 5, respectively. Here one parameter is needed and $W_{-3/2,-5/2}$ which corresponds to the relaxation probability for the transition of the lowest frequency is taken as this parameter. Using these eigenvalues of λ_j, general solution of a_m is given in the following matrix form;

$$\begin{pmatrix} a_m \end{pmatrix} = \begin{bmatrix} 1.00 & 1.00 & 1.00 & 1.00 & 1.00 \\ 1.95 & 1.76 & 1.29 & 0.37 & -1.18 \\ 4.63 & 3.48 & 1.11 & -1.38 & 0.63 \\ 15.68 & 7.64 & -3.02 & 0.74 & -0.14 \\ 127.50 & -10.88 & 1.09 & -0.11 & 0.01 \end{bmatrix} \begin{bmatrix} a_1\exp(-\lambda_1 t) \\ a_2\exp(-\lambda_2 t) \\ a_3\exp(-\lambda_3 t) \\ a_4\exp(-\lambda_4 t) \\ a_5\exp(-\lambda_5 t) \end{bmatrix} \qquad (A,\ 7)$$

where values of $a_1, \ldots\ldots, a_5$ are determined by the initial conditions. In the case of stimulated echo measurement, the initial conditions are the same as in Case 1. Numerical solutions of the relative decay curves of the stimulated echo signal are given by following equations.

For the transition $+5/2 \rightleftarrows +3/2$,

$$a_{+5/2} = 0.568\times 10^{-4}\exp(-\lambda_1 t) + 0.776\times 10^{-2}\exp(-\lambda_2 t) + 0.126\exp(-\lambda_3 t) + 0.665\exp(-\lambda_4 t) + 0.120\times 10\exp(-\lambda_5 t)$$

For the transition $+3/2 \rightleftarrows +1/2$,

$$a_{+3/2} = 0.217\times 10^{-3}\exp(-\lambda_1 t) + 0.241\times 10^{-1}\exp(-\lambda_2 t) + 0.209\exp(-\lambda_3 t) + 0.842\times 10^{-1}\exp(-\lambda_4 t) + 0.168\times 10\exp(-\lambda_5 t)$$

For the transition $-1/2 \rightleftarrows +1/2$,

$$a_{+1/2} = 0.121\times10^{-2}\exp(-\lambda_1 t)+0.940\times10^{-1}\exp(-\lambda_2 t)$$
$$+0.155\exp(-\lambda_3 t)+0.128\times10\exp(-\lambda_4 t)+0.473\exp(-\lambda_5 t)$$

For the transition $-1/2 \rightleftarrows -3/2$,

$$a_{-1/2} = 0.140\times10^{-1}\exp(-\lambda_1 t)+0.453\exp(-\lambda_2 t)+0.115\times10\exp(-\lambda_3 t)$$
$$+0.363\exp(-\lambda_4 t)+0.245\times10^{-1}\exp(-\lambda_5 t)$$

For the transition $-3/2 \rightleftarrows -5/2$

$$a_{-3/2} = 0.924\exp(-\lambda_1 t)+0.919\exp(-\lambda_2 t)+0.149\exp(-\lambda_3 t)$$
$$+0.787\times10^{-2}\exp(-\lambda_4 t)+0.134\times10^{-3}\exp(-\lambda_5 t)$$

These decay curves are shown in Fig.8.

Case 3.

The rate equations are solved in another case when $W_{m,m+1}$ is proportional to $[I(I+1)-m(m+1)]\cdot\omega^4_{m,m+1}$. In this case, λ_j's are given by

$$\lambda_j/W_{-3/2,-5/2} = 1.18,\ 41.12,\ 277.62,\ 1017.70 \text{ and } 2739.61 \qquad (A,\ 8)$$

for j=1, 2, 3, 4 and 5, respectively. The decay curves of the stimulated echo signals are shown in Fig.9.

Table I. The resonance frequencies in ferromagnetic Dy metal.

ransition	resonance frequency (MHz)	transition	resonance frequency (MHz)
Dy^{163}		Dy^{161}	
', +3/2	1979	-5/2, -3/2	1603
'2, +1/2	1570	-3/2, -5/2	1219
'2, -1/2	1162	1/2, -1/2	830
:, -3/2	753	+1/2, +3/2	445
:, -5/2	345	+3/2, +5/2	(60)

Table II. Numerical values of the quantities in (4, 21) and the values of W_o.

Quantity	Numerical value	Unit
Lande factor g_J	4/3	
Nuclear spin I	5/2	
sf exchange integral $2\mathcal{J}$	-0.15	eV
NMR frequency of the transition $-5/2 \rightleftarrows 3/2$ (measured at 1.4°K) $\omega_{-5/2,-3/2}$	2.167×10^9	sec^{-1}
Density of states $N(E_F)$ (for one direction of spin)	27.7/2	Ry^{-1} $atom^{-1}$
Energy gap of spin wave Δ	24	°K
Transition probability		
Theoretical W_o=	$\sim 4 \times 10^2$	sec^{-1} $°K^{-1}$
Experimental W_o=	4.76×10^2	sec^{-1} $°K^{-1}$

Figure Captions

Fig. 1. The line shapes of NMR lines of Dy^{163} in ferromagnetic Dy metal.

Fig. 2. Comparison of experimental and theoretical spin-lattice relaxation decays for all five resonance lines of Dy^{163} in ferromagnetic dysprosium metal. Plots are the experimental values at 1.4°K, while the solid curves are the calculated ones.

Fig. 3. Plots of the observed stimulated echo amplitudes for the center line of Dy^{163} resonance at 1162MHz at 1.4°K and 4.2°K. The abscissa is the time interval between the second and third pulses times absolute temperature.

Fig. 4. Spin-spin relaxation time for the center resonance line of Dy^{163} resonance at 1162MHz.

Fig. 5. Spin wave spectrum in ferromagnetic Dy metal at low temperature calculated by Cooper,. As for the dotted line, see the text.

Fig. 6. The approximated Fermi surface in Dy metal.

Fig. 7. The theoretical spin-lattice relaxation curves for the case 1.

Fig. 8. The theoretical spin-lattice relaxation curves for the case 2.

Fig. 9. The theoretical spin-lattice relaxation curves for the case 3.

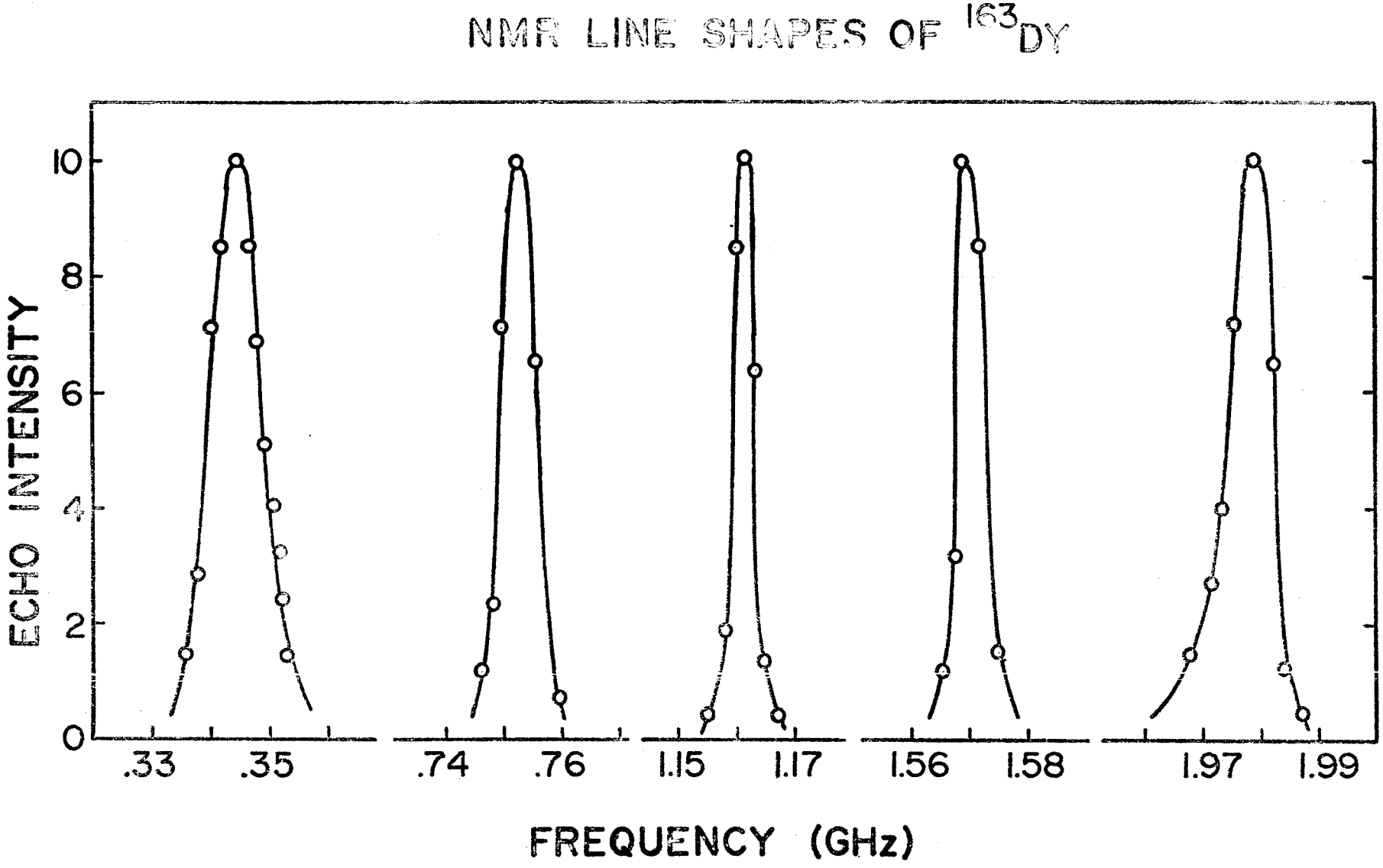
NMR LINE SHAPES OF ^{163}DY
ECHO INTENSITY
0
2
4
6
8
10
.33
.35
.74
.76
1.15
1.17
1.56
1.58
1.97
1.99
FREQUENCY (GHz)

Fig. 1.

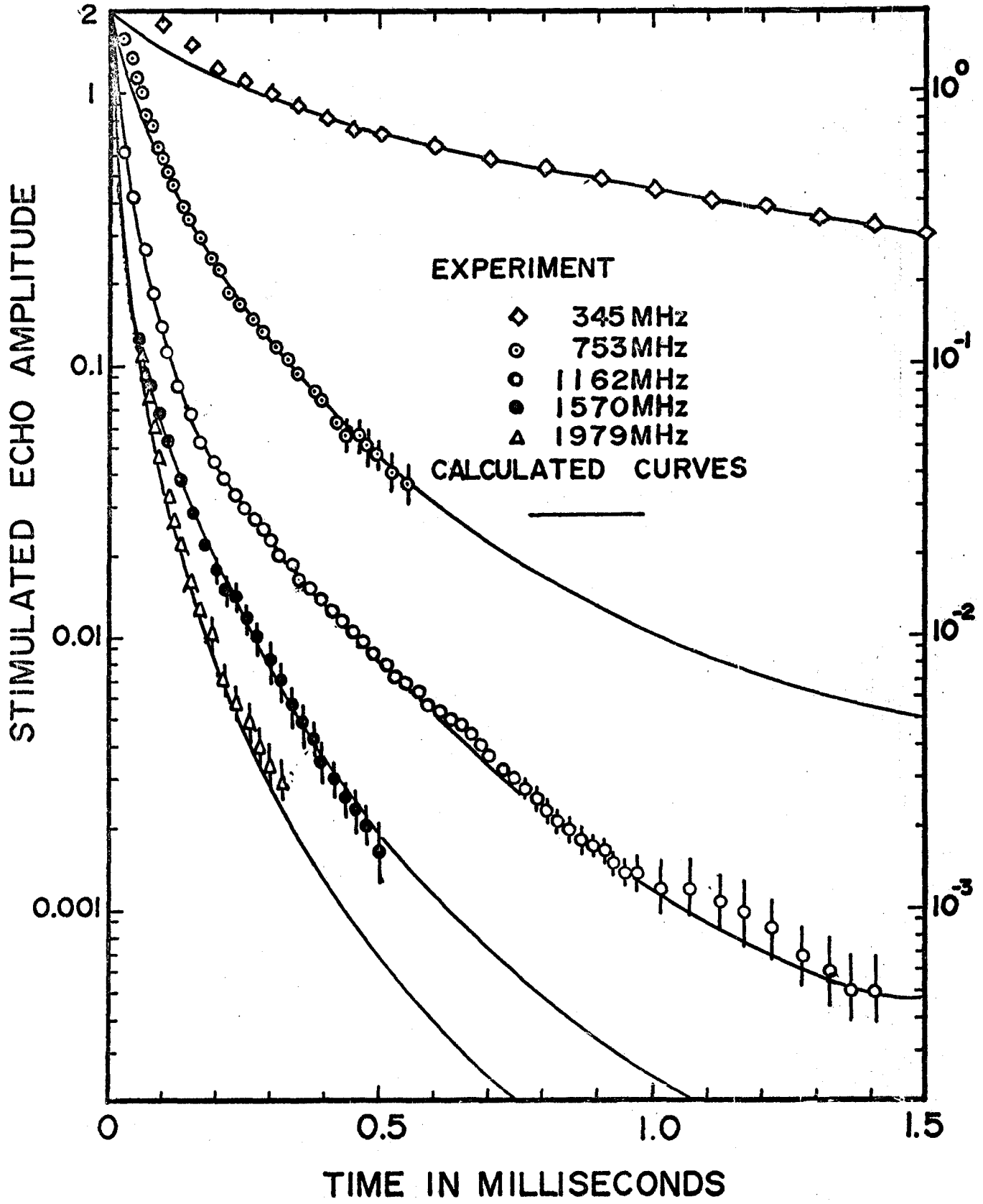
STIMULATED ECHO AMPLITUDE
2
1
0.1
0.01
0.001
10^{0}
10^{-1}
10^{-2}
10^{-3}
EXPERIMENT
345 MHz
753 MHz
1162 MHz
1570 MHz
1979 MHz
CALCULATED CURVES
0
0.5
1.0
1.5
TIME IN MILLISECONDS

Fig. 2.

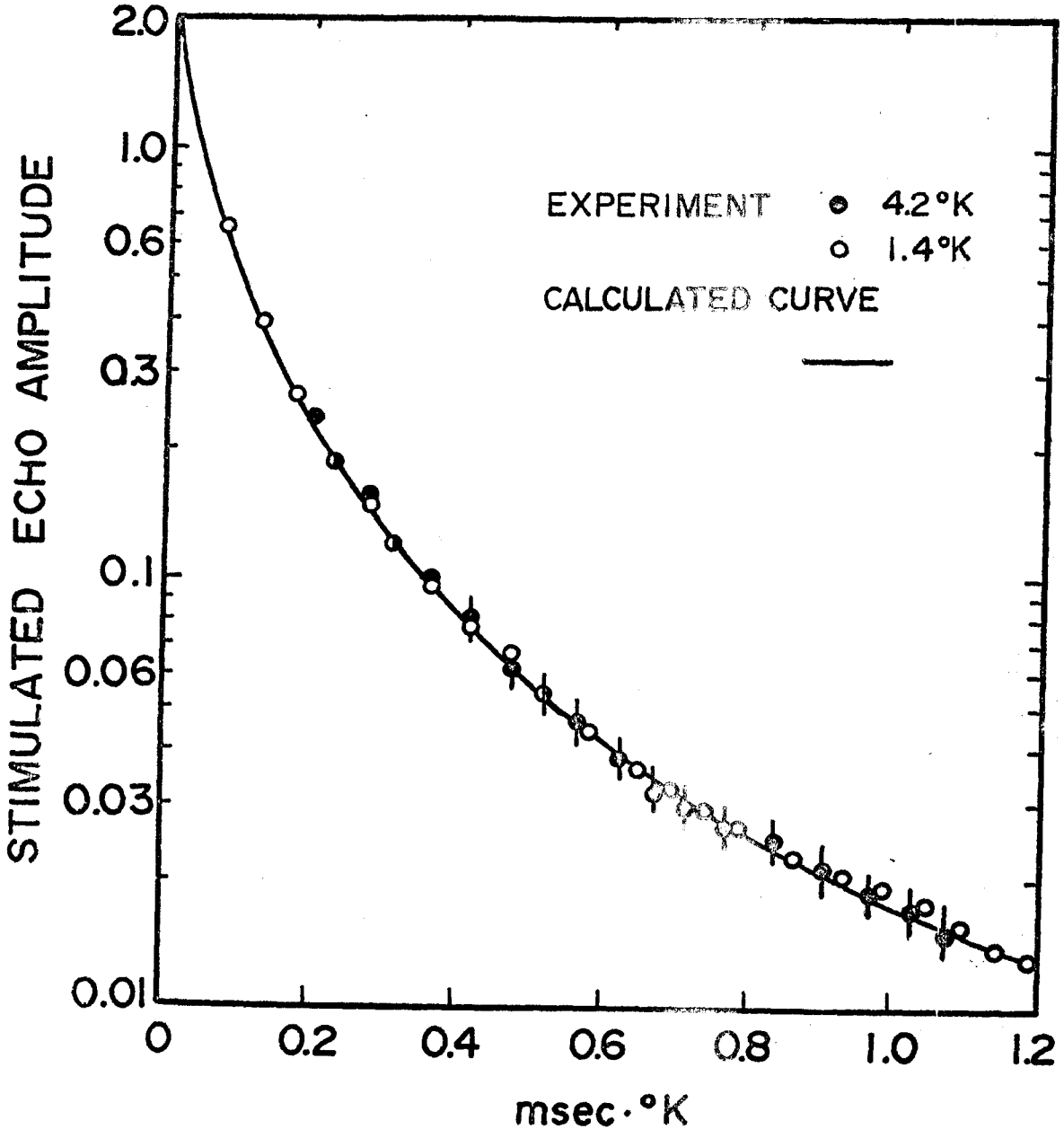
STIMULATED ECHO AMPLITUDE
2.0
1.0
0.6
0.3
0.1
0.06
0.03
0.01
0
0.2
0.4
0.6
0.8
1.0
1.2
msec · °K
EXPERIMENT
4.2°K
1.4°K
CALCULATED CURVE

Fig. 3.

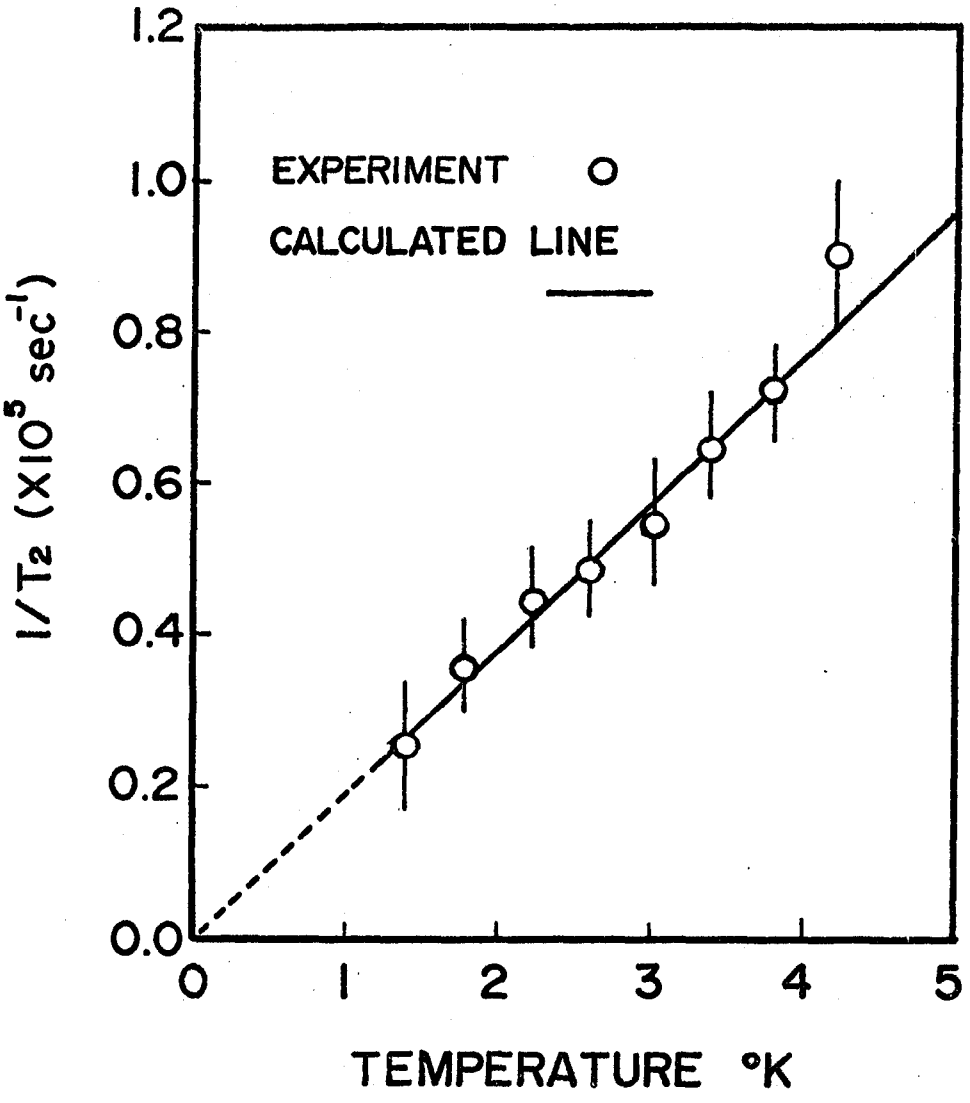
1.2
1.0
0.8
0.6
0.4
0.2
0.0
EXPERIMENT O
CALCULATED LINE
1/T2 (X10^5 sec^-1)
0
1
2
3
4
5
TEMPERATURE °K

Fig. 4.

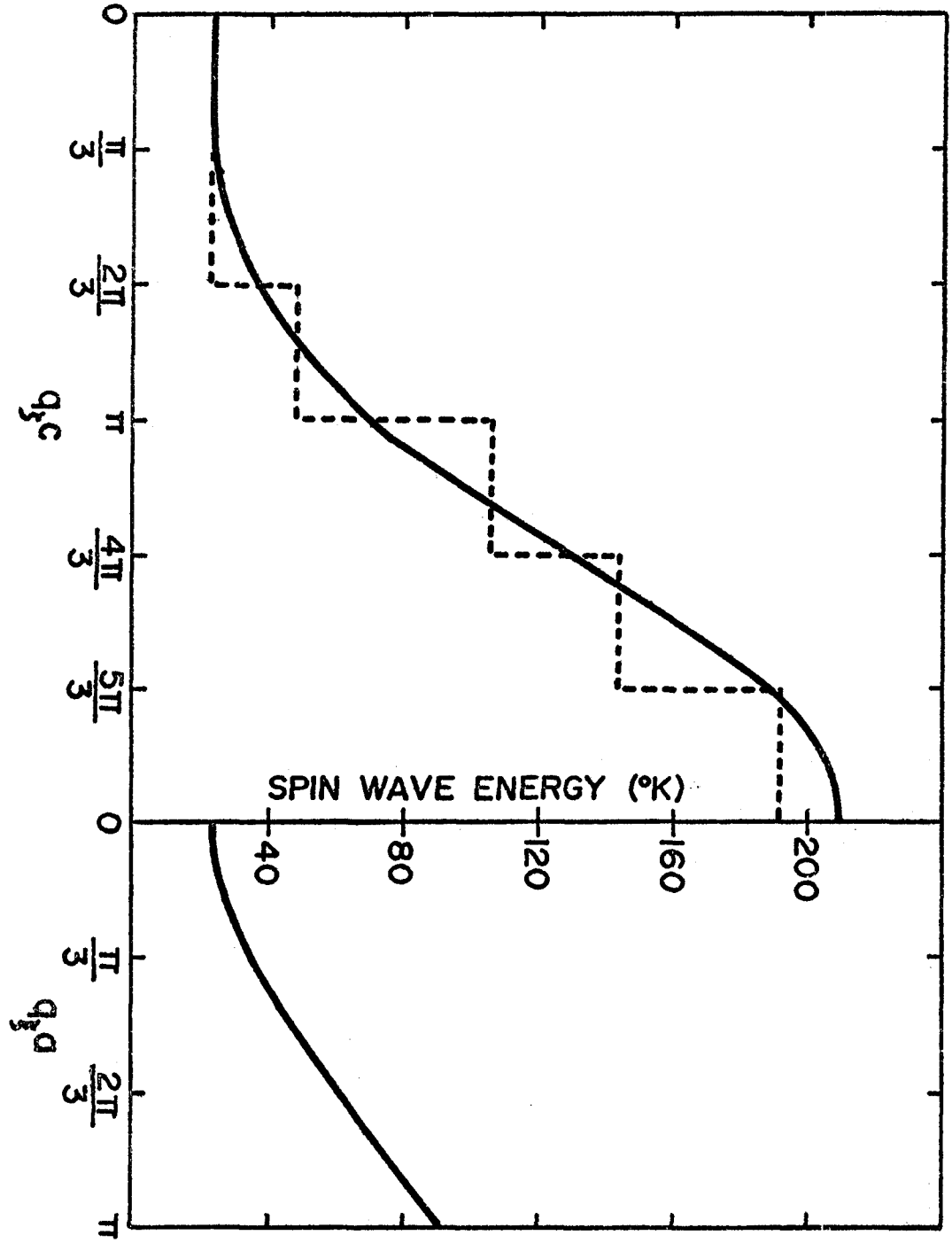
SPIN WAVE ENERGY (°K)
40
80
120
160
200
0
π/3
2π/3
π
4π/3
5π/3
0
π/3
2π/3
π
q_a
q_c

Fig. 5a.

Fig. 5b.

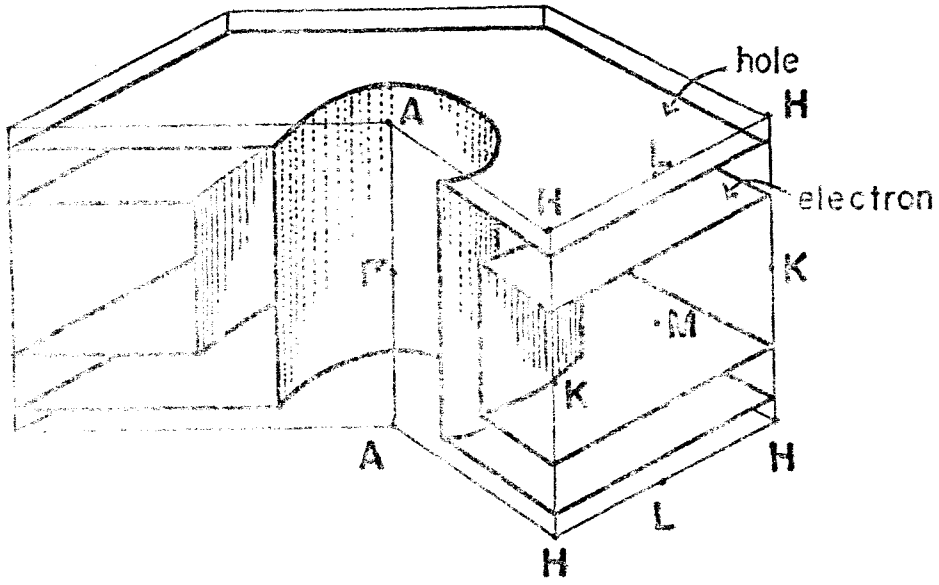
hole
H
A
L
H
electron
K
M
K
A
H
L
H

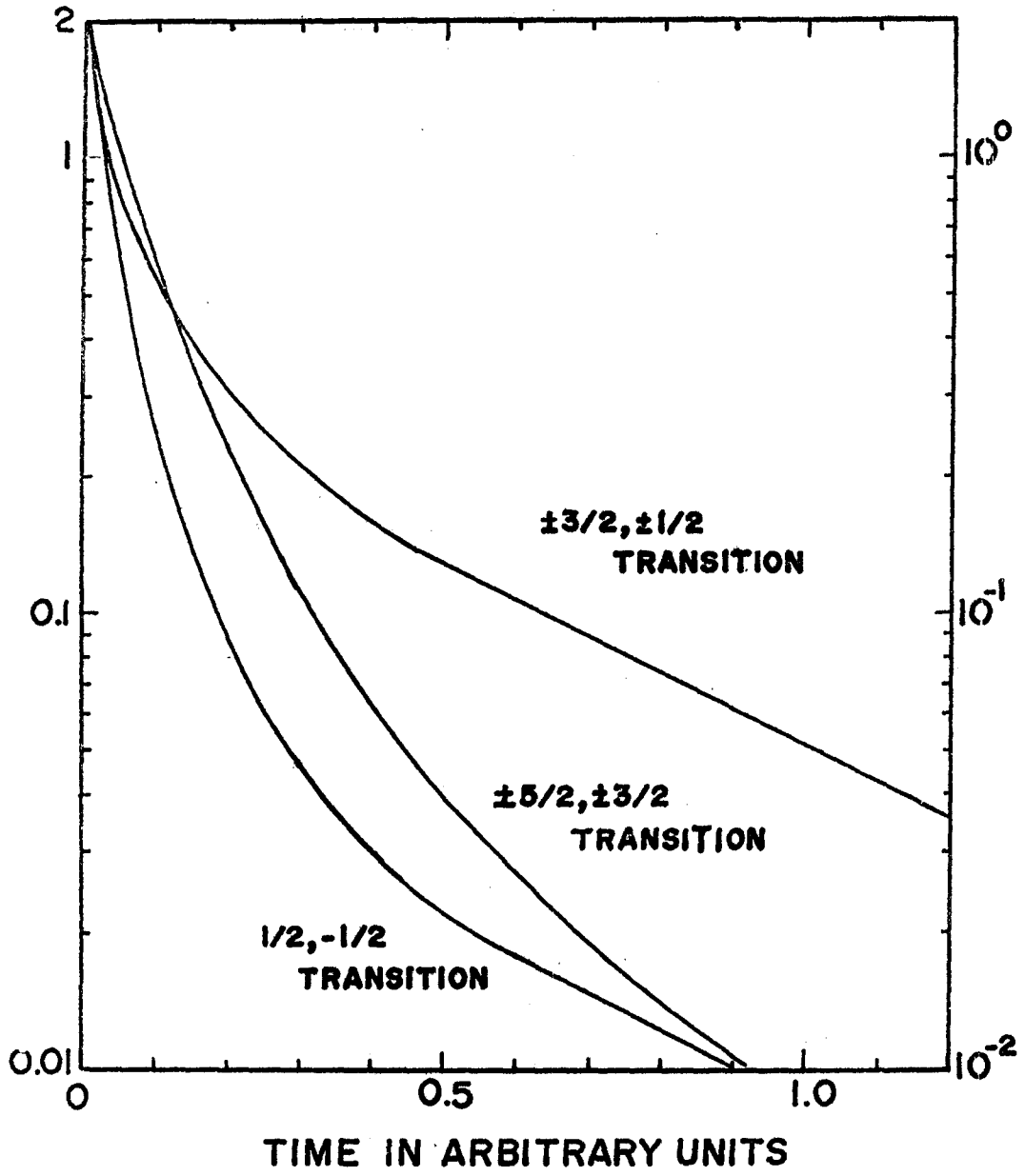
2
1
0.1
0.01
0
0.5
1.0
10^0
10^{-1}
10^{-2}
±3/2,±1/2
TRANSITION
±5/2,±3/2
TRANSITION
1/2,-1/2
TRANSITION
TIME IN ARBITRARY UNITS

Fig. 7

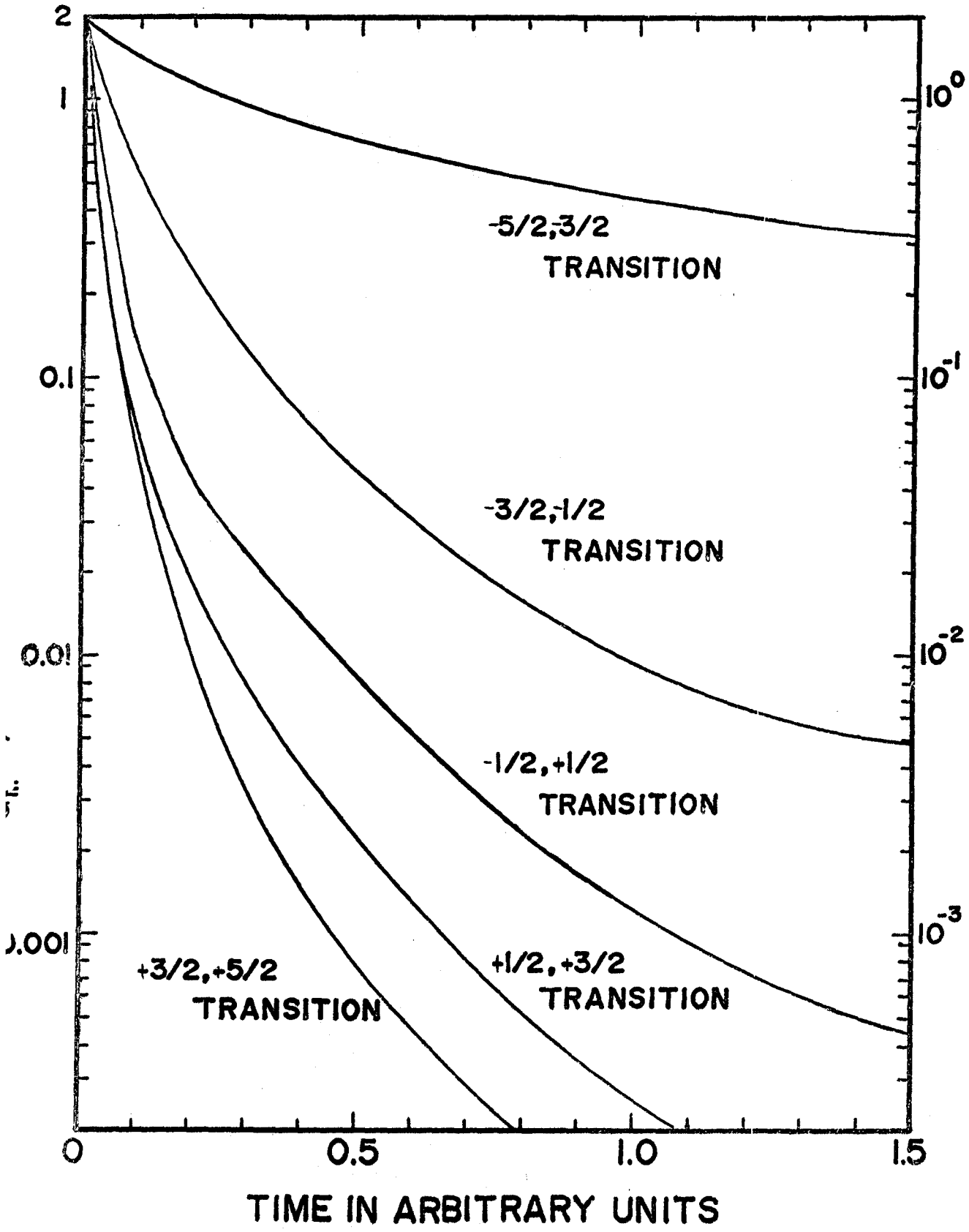
2
1
0.1
0.01
0.001
10^{0}
10^{-1}
10^{-2}
10^{-3}
-5/2,-3/2
TRANSITION
-3/2,-1/2
TRANSITION
-1/2,+1/2
TRANSITION
+1/2,+3/2
TRANSITION
+3/2,+5/2
TRANSITION
0
0.5
1.0
1.5
TIME IN ARBITRARY UNITS

Fig 8.

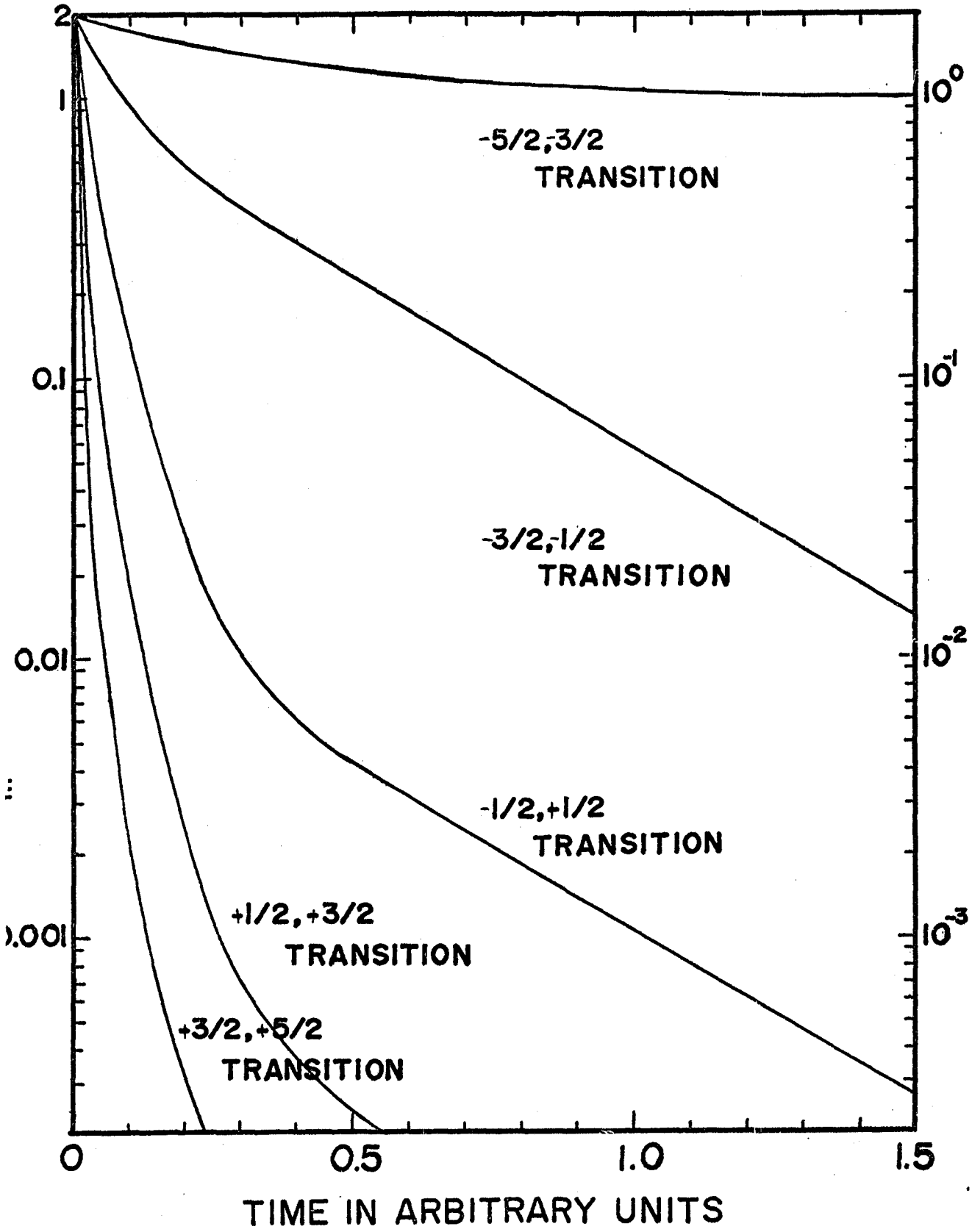
2
1
0.1
0.01
.001
10^{0}
10^{-1}
10^{-2}
10^{-3}
-5/2,-3/2
TRANSITION
-3/2,-1/2
TRANSITION
-1/2,+1/2
TRANSITION
+1/2,+3/2
TRANSITION
+3/2,+5/2
TRANSITION
0
0.5
1.0
1.5
TIME IN ARBITRARY UNITS

Fig. 9

References

1) B. Bleaney: J. appl. Phys. 34 (1963) 1024

2) For Dy metal, D. V. Lounasmaa and R. A. Guenther: Phys. Rev. 126 (1962) 1357.

3) For Dy metal, S. Ofer, M. Rakavy, E. Segal, and B. Khurgin: Phys. Rev. 138 (1965) 241.

4) J. Herve and P. Veillet: CR Acad. Sci. (France) 252 (1961) 99.

5) S. Kobayashi, N. Sano, and J. Itoh: J. Phys. Soc. Japan 21 (1966) 1456.

6) S. Kobayashi, N. SAno, and J. Itoh: J. Phys. Soc. Japan 22 (1967) 676.

7) S. Kobayashi, N. Sano, and J. Itoh: J. Phys. Soc. Japan 23 (1967) 474.

8) J. Kondo: J. Phys. Soc. Japan 16 (1961) 1690; ibid., 17 (1962) 413.

9) J. Itoh, S. Kobayashi, and N. Sano: J. appl. Phys. 39 (1968) 1325.

10) D. Gill and N. Kaplan: Phys. Letters 26A (1968) 505.

11) M. K. Wilkinson, W. C. Koehler, E. O. Wollan, and J. W. Cable: J. appl. Phys. 32 (1961) 49S.

12) A short report was already published, N. Sano, J. Itoh, and S. Kobayashi: J. Phys. Soc. Japan 26 (1968) 857.

13) M. Weger: Phys. Rev. 128 (1962) 1505.

14) R. E. Walstedt: Phys. Rev. Letters 19 (1967) 146, ibid. 816.

15) E. L. Hahn: Phys. Rev. 80 (1950) 580.

16) A. J. Freeman and R. E. Watson: Phys. Rev. 131 (1963) 123.

17) D. L. Uhrich and R. G. Barnes: Phys. Rev. 164 (1967) 428.

18) A. Sher and H. Primakoff: Phys. Rev. 119 (1960) 178,
E. R. Andrew and D. T. Turnstall: Proc. Phys. Soc. (London) 78 (1961) 1.

W. W. Simmons, W. J. O'Sullivan, and W. A. Robinson: Phys. Rev. 127 (1962) 1168.

A. Narath: Phys. Rev. 162 (1967) 320.

19) J. Korringa: Physica 16 (1950) 601.

20) H. Suhl: Phys. Rev. 109 (1958) 606; J. Phys. Radium 20 (1959) 333.

T. Nakamura: Progr. theor. Phys. 20 (1958) 542.

21) Y. Obata: J. Phys. Soc. Japan 18 (1963) 1020.

22) Y. Yafet and V. Jaccarino: Phys. Rev. 133 (1964) A1630.

23) T. Moriya: J. Phys. Soc. Japan 19 (1964) 681.

24) S. C. Keeton and T. L. Loucks: Phys. Rev. 168 (1968) 672.

25) R. J. Elliott and K. W. H. Stevens: Proc. Roy. Soc. A218 (1953) 553, ibid. A219 (1954) 387.

26) T. Holstein and H. Primakoff: Phys. Rev. 58 (1940) 1098.

27) W. Herring et al.: Phys. Letters 28A (1968) 209.

28) A. Narath: Phys. Rev. 178 (1969) 359.

29) B. R. Cooper: Solid State Physics 21 (Academic Press, 1968) 393.

30) H. B. Møller and J. C. G. Houmann: Phys. Rev. Letters 16 (1966) 737.

31) K. A. Gschneidner, Jr.: rare earth research III (Gordon And Breach, 1964) 153.

32) V. Jaccarino, B. T. Matthias, M. Peter, H. Suhl, and J. H. Wernick: Phys. Rev. Letters 5 (1960) 251.

33) R. G. Barnes and E. D. Jones: Solid State Commun. 5 (1967) 285.

34) T. Kasuya: Magnetism IIB (Academic Press, 1966) 215.

S. H. Liu: Phys. Rev. 123 (1961) 470.

35) P. Pincus and J. Winter: Phys. Rev. Letters 7 (1961) 269.

A. Honma: Phys. Rev. 142 (1966) 306.

36) H. Callen and E. Callen: Phys. Rev. 139 (1965) A455.

37) J. F. Smith, C. E. Carlson, and F. H. Spedding: Transactions AIME J. Metals 9 (1957) 1212.

38) S. H. Liu, D. R. Behrendt, S. Legvold, and R. H. Good, Jr.: Phys. Rev. 116 (1959) 1464.
J. J. Rhyne and A. E. Clark: J. appl. Phys. 38 (1967) 1379.

39) A. E. Clark, B. F. DeSavage, and R. M. Bozorth: Phys. Rev. 138 (1965) A216.

40) D. Sherrington: J. Phys. C, Proc. Phys. Soc. (Solid State Phys.) 1 (1968) 748.

41) A. Abragam: The Principles of Nuclear Magnetism (Oxford University Press, 1961)

PART II

Nuclear Magnetic Resonance and Relaxation of ^{159}Tb in Ferromagnetic Terbium Metal

Abstracts.

Nuclear magnetic resonance and relaxation phenomena of ^{159}Tb have been investigated by spin echo technique at liquid helium temperatures. The nuclear magnetic resonance spectrum consists of three equally spaced lines in the frequency range from 2.4GHz to 3.9GHz. The center line frequency corresponding to the Zeeman energy is 3120MHz and the frequency difference of the adjacent lines corresponding to the quadrupole effects is 673.5MHz. In the spin-lattice relaxation, it is concluded that the relaxation process is the same as that in ferromagnetic dysprosium metal. The spin-spin relaxation time is determined by the spin-lattice relaxation and the I·I coupling.

I. Introduction

Among the elements in the second half of the rare earth series, terbium and dysprosium have the hexagonal close-packed structure and are ferromagnetic below 222K and 85K, respectively, with a large axial anisotropy which has the effect of holding the magnetization in the hexagonal basal plane.

The purpose of this paper is to present experimental results of the nuclear-magnetic-resonance (NMR) and nuclear-magnetic relaxation in ferromagnetic terbium metal at liquid helium temperatures. A set of similar experiment and calculation of the relaxation has been carried out for ferromagnetic dysprosium metal in Part I. In both cases of terbium and dysprosium the hyperfine interactions produced by the unfilled shell of 4f electrons are dominant and the main origin in the spin-lattice relaxation mechanism is the Weger's mechanism[1] which has been described in the section IV-2 of Part I.

The observation of the hyperfine interaction in ferromagnetic terbium metal have been done by nuclear specific heat measurments[2] and Mössbauer studies[3]. Though the accuracy of these measurements is not good, these data agree with the present experimental results. The first NMR observation in ferromagnetic terbium metal was reported by Herve and Veillet[4], but their observation was not well reproducible and could not be ascribed with certainty to NMR in terbium.

In following sections, the experimental techniques used in the present work and the experimental results are described. Also, the discussions with numerical estimation are presented in relation to

the hyperfine interactions, the spin-lattice relaxation, and the spin-spin relaxation. For the case in which the spin-lattice relaxation process is mainly determined by the Weger's mechanism, the solution of rate equations which describes the decay behavior at low temperature is given in Appendix.

II. Experimental Techniques

Throughout the present work, ingot terbium metal specimen from commercial source, Materials Research Corporation, was used. According to the supplier, the purity was better than 99.7 % and principal impurities were (in %), Y-0.1, Ta-0.1, O-0.04, Fe-0.02, Si-0.02, Ca-0.02, and Cu-0.02. Sample used in the NMR measurements were prepared by filing the ingot into powder form with a few ten microns in diameter. No care was paid to avoid oxidization and the powders probably were covered with oxide, by which each powder was electrically insulated from others. The NMR signals at considerably later days from the filing gave the same resonance frequencies and line shapes as compared to those obtained just after the filing indicating that there was no trouble about sample treatment.

The spin echo apparatus in ultra high frequency (UHF) range was in principles the same as that developed already by Kobayashi[5]. In the present work, we constructed the high power spin echo apparatus for UHF range from 2GHz to 4GHz. Figure 1 shows the block diagram of the system, which is the same as that of conventional pulse spectrometer. The 1G45P hydrogen

thyratron tubes were used with delay lines to produce negative DC square pulses up to 1 kilovolt. The delay line was adjusted to make a pulse of 1 μsec width and to have an impedance of 50Ω to be matched to the input impedance of a pulse transformer. In the present case, it was designed to get three 90° pulse sequences. The pulse-transformer transformed the voltage and polarity of negative DC pulses up to 4.5 kilovolts and the impedance to match that of the tube used in the reentrant oscillator.

A lighthouse-tube reentrant cavity oscillator for pulse operation is shown in Fig. 2. In this oscillator there was cylindirical conductor connected to the cathode, a concentric tube connected to the anode cap, and a short open-ended cylinder connected to the grid disk. The cathode and plate cylinders were connected by a short-circuiting plunger of a choke type. The output probe was located in the region between the grid and cathode cylinders; the depth of penetration was adjusted by means of a threaded collar. To tune the oscillator the entire asembly could be moved on or off the anode cap of the tube by means of a tuning knob. A quarter-wavelength cup forming a plate choke plunger was adjusted by means of tuning rods to obtain optimum condition. We prepared many grid cylinders and plate choke plungers to cover the frequency range from 2GHz to 4GHz. The 2C43 lighthouse tubes were used up to 3.5GHz and the 2C40 lighthouse tubes were used from 3.5GHz to 4GHz.

The sample cavity shown in Fig. 3 approximated a three-quarter-wavelength short-circuited coaxial line and it was

immersed directly in liquid helium. To cover the frequency from 2GHz to 4GHz, three cavities of different lengths was constructed with the same design. As shown in Fig. 3, the cavity was tuned by varying the length of the center conductor. Contact fingers were placed at low-current region, approximately one-quarter wavelength apart from the short-circuited end of the cavity. The effective position of the fingers varies with frequency, however, and each of the three cavities was designed so as to keep the fingers always in a low-current region at desired frequencies. Also, the cavity had coupling loops for input and output of powers which were designed to cover a wide frequency range without unreasonable variations in Q and transmission loss. Samples were put into the top position of the sample cavity through a small hole.

A PIN diode that was mounted in a coaxial cavity was used to prevent burning-out of the 1N23C crystal used for the mixer. This PIN diode was operated by the gated pulse and only the echo signal could pass to the mixer. In the 2.4GHz range, a 2C40 lighthouse tube grid-separation oscillator was used for the local oscillator. The 726A and 2K29 klystron oscillators were used for the local oscillators in the 3.1GHz and 3.8GHz ranges, respectively. Only the echo signal was converted into 60MHz by the crystal mixer, and was amplified by a conventional intermediate amplifier with the center frequency of 60MHz and the band width of 3MHz.

The NMR line shapes of terbium metal were determined by point to point plots of the echo intensities when the frequency

of the rf pulses was varied with every two or three MHz step. Each point was an average of several repeated observations. In each one measurement of echo height it was necessary to adjust the frequencies of the oscillators and the resonance condition of cavity resonators. In narrow frequency range the measurement of relative intensities of echo signals was reliable, but because the calibrations of the sensitivity of the apparatus and of the rf power of the pulse oscillators were quite difficult in widely different frequency ranges the relative intensities of lines which correspond to different transitions could not be obtained in any accuracy.

The spin-lattice relaxation was measured by stimulated echo method[6]. (Typical stimulated echoes are shown in Fig. 4.) In the case of Tb the NMR spectrum consists of three lines with widely different frequencies, which are due to a large quadrupole interaction. Therefore a rf pulse can induce only one transition among three. As will be discussed in latter section, the relaxation decay is not simply exponential in this case, and the whole decay curve had to be measured to analyze it to compare with the theory. For this purpose, the stimulated echo method seems to be the best. Because of broad line shape, it was impossible to disturb whole spins belonging to one line by a rf pulse with single frequency, but only a hot spot will be produced at the frequency of the pulse. The observed decay corresponds to the decay of this hot spot.

The spin-spin relaxation was measured by the change of the echo height when the separation time of two 90° rf pulses

which produce the echo was varied. Because the spin-spin relaxation time is very short, the accurate determination of the spin-spin relaxation time was rather difficult.

The magnetic isotope of terbium is ^{159}Tb which has spin I=3/2 and whose natural abundance is 100%. The NMR measurement was done at liquid helium temperatures between 1.35K and 4.22K. The temperature was controlled by regurating pumping rate of helium gas in the Dewar vessel. Because the power of rf pulses was strong and the relaxation rate is a function of temperature, care was taken to keep good thermal contact between the sample and the liquid helium; powder sample contained in an open glass tnbe was directly immersed in liquid helium. To assure the thermal equilibrium at the beginning of the measurement, the repetition time of the measurement was chosen to be longer than 400msec which is much longer than the spin-lattice relaxation time.

III. Experimental Results

III 1. Nuclear-Resonance Line Shape

The shapes of the resonance lines of ^{159}Tb are shown in Fig. 5. The principal feature of these line shapes is that each line corresponding to the transition $m \leftrightarrow (m+1)$ has two satellite lines beside a strong main peak. The frequency of the main peak in $(-\frac{1}{2}) \leftrightarrow (+\frac{1}{2})$ transition, which corresponds to the Zeeman frequency of the main line, is 3120MHz and the frequency difference of the main peaks of the adjacent lines, ν_Q, which corresponds to the quadrupolar frequency, is 673.5MHz.

The spin-spin relaxation time of the satellite line, S_1, which is observed in low frequency side of each main line is about one order of magnitude smaller than that the corresponding main line. On the other hand, the spin-spin relaxation time of the satellite line, S_2, in high frequency side of the main line, is of the same order of magnitude as that of the corresponding main line. The enhancement of NMR is not different for S_1 and S_2 lines from that for the main line. Therefore three S_1 lines form a set and three S_2 lines form a different set. The Zeeman frequencies and the quadrupolar frequencies of these satellite lines are different from those of the main line as shown in Table I.

TABLE I

The NMR Frequencies of ^{159}Tb in Ferromagnetic Terbium Metal

The frequencies are given in MHz at 1.35K.

Transition	Resonance Frequency		
	Main Line	Satellite Line	
		S_1	S_2
-1/2 -3/2	2447	2433	2500
(ν_Q)	(673)	(664)	(700)
-1/2 +1/2	3120	3097	3200
(ν_Q)	(674)	(665)	(680)
+1/2 +3/2	3794	3752	3880

With similar arguments to the case of NMR of Dy metal which have been described in Part I, it is certain that the main lines corresponds to the NMR of Tb nuclei in bulk domain of Tb metal, while the satellites may arise from Tb nuclei in domain wall of the metal or Tb nuclei in some impurity compounds contained in our samples. Possible origins of the satellites will be discussed in later section. In any case, the satellite lines are very much weaker than the main line and have little effect on the relaxation measurements of the main line.

Detailed measurements of the spin-lattice relaxation and the spin-spin relaxation which will be described in the following were done only for the main lines.

III 2. Spin-Lattice Relaxation

Fig. 6 shows the decay curves of the stimulated echo amplitudes for all three main resonance lines of ^{159}Tb in ferromagnetic terbium metal plotted against the time interval between the second and third pulses, at 1.35K. The decay curves were measured at a few temperatures between 1.35 and 4.22K. As shown in Fig. 7, the decay curves of the 2447MHz line measured at 4.22K and 2.58K coincide with that measured at 1.35K when the intensities of the stimulated echos are plotted against tT^* (t is the time interval between the second and third pulses and T is the absolute temperature.) This result indicates that the spin-lattice relaxation probability is proportional to absolute temperature.

* In the case of the NMR in ^{159}Tb, the Zeeman energy is so large that, strictry speaking, the high-temperature approximation in the calculation of rate equations of spin-lattice relaxation cannot be applied and it is expected that the decay curves obtained at 4.22K don't coincide exactly with that obtained at 1.35K in such plots. But, as discussed in the later section and appendix, the difference between the results of exact calculation and high-temperature approximation is still small at 1.35K and is less than or of the order of the experimental errors. The decay measurement at still lower temperature seems interesting.

When a fraction of the spins are selectively excited by an rf pulse, then, due to spin-spin coupling, the excitation would spread out to other spins which are not excited by the rf field. Spin diffusion to different frequencies, that is the spectral diffusion, can, in principle, be investigated by saturating a portion of the spectrum, and observing the rate of the recovery to the thermal equilibrium within the spin system by the spin-spin interaction[7]. However, it is very difficult to use this method for the investigation of spectral diffusion.

The stimulated echo technique provides a quantitative mean of investigating spectral diffusion. According to Hahn's calculation[6], the decay of the stimulated echo is proportional to $\exp(-t/T_1)\cdot\exp(-k\tau^2 t)$, where t is the time interval of two spin echoes, T_1 is the spin-lattice relaxation time, τ is the

time between two pulses which produce the first echo, and k is the probability of spectral diffusion which is probably independent of temperature. If the spectral diffusion were appreciable, the stimulated echo hight would depend upon τ. In the present work, though only a hot spot produced by the rf pulses was observed in our experiment, the decay curve of the stimulated echo is proportional to absolute temperature and the plots of the decay curves with widely different values of τ coincides with each other as shown in Fig. 8. These experimental results suggest that the effect of spectral diffusion is quite negligible in ferromagnetic terbium metal.

The decay of the stimulated echo shown in Fig. 6 is not simply exponential. This is the feature of the relaxation of NMR lines split by quadrupole interaction. The decay curve is the sum of three exponential curves when I=3/2 as described in Appendix of Part I. The time constant of each exponential function can be calculated by solving rate equations for the occupation probabilities of nuclear levels, and depend upon what is the dominant relaxation mechanism. In Appendix, we show the solution of the rate equations when the relaxation probability is proportional to $(I-m)(I+m+1)\omega^2_{m,m+1} \cdot T$ corresponding to the relaxation mechanism shown in Sec. IV.2 of Part I. In calculating decay curves, only one parameter is needed, and for this parameter we take W_o which is equal to $W_{-3/2,-1/2}/T$ where $W_{-3/2,-1/2}$ is the relaxation probability between two lowest levels. Because $W_{-3/2,-1/2}$ is proportional to T, W_o is independent of temperature. Taking a value 4.58×10^3 $sec^{-1} \cdot K^{-1}$ for W_o, we compare the observed

plots of the decay of the stimulated echo signals shown in Fig. 6 with the calculated decay curves which is shown in the same figure and it is found that the agreement between the experimental plots and the calculated curves is quite satisfactory. Thus it was found that the spin-lattice relaxation probability $W_{m,m+1}$ is proportional to $(I-m)(I+m+1)\omega^2_{m,m+1}T$ like that of the ferromagnetic dysprosium metal.

III 3. Spin-Spin Relaxation

Contrary to the case of the stimulated echo signal, the decay of the echo signal which is produced by two 90° rf pulses follows a simple exponential function as the time interval, τ, between the two pulses increases. Hence the spin-spin relaxation time, T_2, is measured directly by plotting the logarithm of the echo heights versus the twice of this time interval. We have measured the temperature dependence of T_2 in liquid helium temperature range and the results is shown in Fig. 9. Because of fast decay, the accurate determination of T_2 was rather difficult and the observed values of T_2 fluctuate a little for different series of measurements. Circular plots shown in Fig. 9 are the average values of repeated measurements at the same temperature and the virtical line at each plot indicates a probable error.

Fig. 9 shows that T_2 contains a term which is proportional to 1/T and a term which is independent of T. Because the spin-spin relaxation arising from Suhl-Nakamura interaction[8] is generally independent of temperature, and also that the spin-

lattice relaxation probability is found to be proportional to T as already described, this result suggests that the observed T_2 can be divided into two parts; one is determined by spin-lattice relaxation and another is determined by the spin-spin relaxation which is independent of temperature. The former part will be calculated by the use of the Walsted's theory[9] which was described in Sec. IV-3 of Part I and this temperature dependent parts are shown in Fig. 9 with solid lines for all three transitions. The temperature independent parts for the transitions between $m=\pm 1/2$ and $\pm 3/2$ are about twice as large in magnitude of $1/T_2$ as that for the transition $m=+1/2 \leftrightarrow -1/2$.

IV. Discussion

IV 1. Hyperfine Interactions

The large magnetic dipole and electric quadrupole hyperfine energies of ^{159}Tb in ferromagnetic terbium metal are mainly due to the hyperfine interaction arising from the unfilled 4f electrons of Tb^{+3} ions in the metal. As the spin and orbit are strongly coupled in the trivalent ion, the principal axis of the electric field gradient (EFG) produced by J will be parallel to the direction of the electronic magnetization. Taking this as the z-axis, if any contribution from conduction electrons and core polarization is neglected, the Hamiltonian would have the form, as described in Part I.

$$\mathcal{H} = AJ I_z + P\left\{I_z^2 - \frac{1}{3} I(I+1)\right\}, \qquad (4.1)$$

where

$$P = -B\langle 3J_z^2 - J(J+1)\rangle = -BJ(2J-1), \qquad (4.2)$$

and A, B are already described in eqn (4.2) of Part I. This hyperfine interaction constants, A and B, for the rare-earth metals were estimated independently by Bleaney[10] and Kondo[11]. The calculated values are in agreement with our NMR data on terbium, dysprosium, and erbium metals as shown in Table II. These results show that in the co-operative magnetic state the rare-earth ions in metals can be rather exactly described as the tripositive ions whose saturated moment corresponds to $J_z=J$.

TABLE II

NMR data at 1.35K for the metals and calculated values for the free tripositive ions. AJ and 2P are corresponding to the magnetic dipole and electric quadrupole hyperfine constants, respectively.

Ion	Magnetic Structure	Isotope	Abundance (%)	I	AJ (MHz) (Calc.)[a]	AJ (MHz) (Exp.)	2P (MHz) (Calc.)[a]	2P (MHz) (Exp.)
65 Tb^{3+}	Ferro.	159	100	3/2	+3180	3120	+720±30	673.5
66 Dy^{3+}	Ferro.	161	19.0	5/2	-820±20	830	+300±60	386
		163	24.9	5/2	+1140±20	1162	+360±60	409
68 Er^{3+}	Cone	167	22.9	7/2	-940	906[b]	-136	103[b]
						913[b]		

a Reference 10

b Reference 12

There are other possible contributions to the hyperfine interactions arising from various origins as discussed in Part I. If it is assumed that the magnetic field at the nucleus in ferromagnetic metal produced by core polarization is the same as that in paramagnetic salt which was estimated by Bleaney[13], this value is about -234MHz for ^{159}Tb and is considerably small compared with the observed value of 3120MHz, or about 7.5%.

The contribution from the polarization of conduction electrons to the magnetic field has a long range character[14] as described in Part I. If it is assumed that this polarization is uniform, this contrinution is about -336MHz for ^{159}Tb and is comparatively small, or about 10%.

As presented in Sec. III, the NMR corresponding to the Zeeman transition of ^{159}Tb consists of one main line and two satellite lines. The main line is the NMR of terbium nuclei in bulk domain and the satellite line S_1 may be the NMR in domain wall. The domain structure of ferromagnetic heavy rare-earth metals have not been studied. In contrast to ferromagnetic 3d transition metals, the enhancement of NMR in domain wall of ferromagnetic heavy rare-earth metals seems to be of the same order of magnitude as that in bulk domain by following reasons. In the ferromagnetic structure of terbium metal, there is a very strong anisotropy which acts to keep the moments parallel to the hexagonal planes in which a smaller anisotropy favors magnetic ordering along a $\langle 10\bar{1}0 \rangle$ direction, or the b-axis[15]. The large magnetocrystalline anisotropy demonstrates a strong coupling between the magnetic moments and the lattice. It has been shown that a structure

change from hexagonal to orthorhombic take place[16] in the ferromagnetic state. This distortion involves relative change in linear dimensions as large as 4.6×10^{-3} for $\Delta b/b$. This observed magnetostriction is larger by almost two orders of magnitude than that in ferromagnets such as iron, nickel, and cobalt. It is the consequence of these facts that the domain wall is probably difficult to enhance the NMR. The origin of the change of Zeeman energy of the satellite line S_1 from that of the main line is not certain but may be due to the difference in the conduction electron polarization.

The change of Zeeman energy of the satellite line S_2 is larger than that of the satellite line S_1. Because the NMR line shape of ^{159}Tb was not change in Tb_{90}-Y_{10} (as shown in Fig. 10), Tb-Gd, and Tb-Dy alloys[14], the impurities in the sample may have nothing to do with the satellite line S_2. The NMR of the ferromagnetic compounds which might be formed in the course of our sample preparations, for example TbN[17], may be the origin of S_2. However, by the compound which was formed by heating terbium metal under N_2 atmosphere for a long time, no resonance was observed in this frequency range. As the Néel temperature of the antiferromagnetic compound, Tb_2O_3[18], which might be contained in our powder sample is 2.4K, the NMR of Tb_2O_3 may not probably be observed at the present experimental temperature in this frequency range. Other possible origin of the satellite line S_2 may be the admixture of excited states with different J through the crystal field for Tb nuclei in lattice imperfection. However, this

too may be unprobable, because the excitation energy for different J states is quite large. Therefore the origin of S_2 satellite is un-known at present stage.

Now, we shall discuss the quadrupole interaction in ferromagnetic terbium metal. The quadrupole hyperfine interaction is mainly due to the electric field gradient (EFG) produced by J which is described in eqn (4.2). In terbium metal, as the electron moments lie normal to the hexagonal axis at low temperature, the quadrupole interaction must be modified by including a term $P'(I_x^2-I_y^2)$, where P' is proportional to $\langle J_x^2-J_y^2\rangle$ [19]. Here, the z-axis is chosen in the direction of magnetization. Taking the hexagonal axis as the x-axis, we have $\langle J_x^2\rangle=0$, $\langle J_z^2\rangle=J^2$, giving $\langle J_y^2\rangle=J$. Hence

$$P'/P = -1/(2J-1) . \qquad (4.3)$$

Since P' is essentially an off-diagonal term, its effects are of order $(P')^2$ and the central hyperfine resonance line may be displaced by less than 1MHz, and the outer lines by still less, both being less than the experimental error.

Bleaney[10] estimated the quadrupole hyperfine interaction produced by J to be, P=360MHz, namely $q(4f)=-36.8\times10^{24}cm^{-3}$. Here no Sternheimer correction[20] is included.

In addition to the EFG at the nucleus due to the 4f electrons, there will be the contributions in the metal from the lattice and the conduction electrons. The crystal structure of terbium metal is the hexagonal structure but terbium metal shows an orthorhombic distortion[16] corresponding to an expansion along

the b-axis or $\langle 01\bar{1}0 \rangle$, the easy direction of magnetization in terbium, below its temperature of ferromagnetic ordering, 222K. In this case the contribution to P from the lattice is then

$$P(\text{lattice}) = -\frac{3e^2Q\,q(\text{lattice})}{4I(2I-1)}[1-\eta\cos 2\varphi][1-\gamma_\infty] \quad (4.4)$$

where, $\eta=(V_{XX}-V_{YY})/V_{ZZ}$ and γ_∞ is the Sternheimer shielding (anti-shielding) factor. The observed orthorhombic distortion[16] amounts only to 0.8% at 77K, so η may be negligible. The lattice sums required for an evaluation of the hcp EFG have been calculated by deWette[21] as a function of c/a ratio using the plane-wise summation method. The calculated value of P(lattice) is -9.0MHz using $Q=+1.12\ 10^{-24}cm^2$. The calculated value is based on point charge model with Z=+3, and Sternheimer factor of -75. The lattice constants were taken to be a=3.586Å and c/a=1.593 for hcp terbium metal[16] at 77K. This contribution to the EFG is quite small. The contribution to EFG from the non-s character of the conduction electrons seems difficult to be estimated, but in paramagnetic thurium metal this contribution has been obtained[22] as already described in Part I. Namely, it has been shown that the contribution to EFG from the conduction electrons has same order of magnitude as that from the lattice. Though the value is not measured in terbium metal, that may be of about the same magnitude in terbium metal as in thurium metal. Thus the contribution to EFG from the 4f electrons is the main part as in the case of the magnetic hyperfine interaction.

The difference in the quadrupole interactions of the satellite

line S_1 which arise from the nuclei in domain wall from that of the main line cannot be understood at the present stage. As for the satellite line S_2, nothing can be discussed.

IV 2. Spin-Lattice Relaxation

In this section, we apply the theory developed in Sec. IV of Part I to the experimental relaxation rate of ferromagnetic terbium metal. Because of the large number of parameters which are contained in the numerical estimation of the theoretical transition probability and are not known accurately, it is, of course, hopeless to obtain an accurate theoretical value which can be compared with the experimental relaxation rate. Our aim is to calculate theoretically the order of magnitude of the relaxation rate and show that the relaxation mechanism proposed in Sec. IV-2 of Part I is dominant also in ferromagnetic terbium metal.

Before entering the discussion of the relaxation mechanism described in Sec. IV-2 of Part I, we first consider briefly the Korringa mechanism. The transition probability $W^{(K)}_{m,m+1}$ between the nuclear levels m and m+1 by Fermi contact interactions of the conduction electrons was given by the equation (5.1) of Part I. The quantity of the density of the conduction electron on the Fermi surface at the nuclear site is not obtained in terbium metal, but it was estimated for lanthanum metal from the measurement[23] of the Knight shift. Assuming that the Knight shift in terbium metal is not so much different from that in lanthanum metal, which can be considered to be different from

heavy rare-earth metals only in the point that it does not have 4f electrons, we can use the Knight shift in lanthanum metal to evaluate the $W^{(K)}_{m,m+1}$, giving

$$W^{(K)}_{-3/2,-1/2}/T \simeq 1.3\times10^{-1}\,\mathrm{sec}^{-1}.\mathrm{K}^{-1}$$

This Korringa relaxation probability is two orders of magnitude smaller than the experimental value. Because $W^{(K)}_{m,m+1}$ is independent of the resonance frequency, $\omega_{m,m+1}$, the decay curves expected from this process are entirely in disagreement with the experimental curves. Therefore, the Korringa mechanism is entirely negligible.

One more possible relaxation mechanism which arises from magneto-elastic coupling will be discussed next. The relaxation probability by this mechanism was given by the equation (5.3) of Part I. The evaluated value is given by

$$W^{(m,e)}_{-3/2,-1/2}/T \simeq 2.5\,\mathrm{sec}^{-1}.\mathrm{K}^{-1}.$$

This result is about three orders of magnitude smaller than the experimental value. Thus the contribution of this process to the relaxation is quite negligible.

We now return to the main relaxation mechanism, in which the nuclear energy relaxes to the kinetic energy of the conduction electrons via spin waves. This process was already calculated in Sec. IV-2 of Part I and the relaxation probability was given by the equation (4.21) of Part I. To evaluate the relaxation probability, values of various quantities contained in the equation (4.21) of Part I should be known. We first discuss these.

Møller and Houmann[24] reported measurements of the spin-wave spectrum in ferromagnetic terbium metal by inelastic neutron scattering. The results at 90K for wave vector q along the principal symmetry direction in reciprocal lattice space are shown in Fig. 11. Gooding[25] analysed the neutron scattering data and calculated the spectrum at absolute zero temperature. On comparison of the spin-wave spectra in terbium and in dysprosium described in Sec. V of Part I, the spin-wave energy at q=0 in terbium turns out to be larger than that in dysprosium. Its value is about 30K. And the constant D in eqn (5.2) of Part I is slightly larger than that in dysprosium. If it is assumed that the shape of the Fermi surface of terbium metal is not so much different from that of dysprosium metal calculated by Keeton and Loucks[26], we can approximate the Fermi surface of terbium to that shown in Fig. 6 of Part I. The numerical value of the integral in eqn (4.21) of Part I, in case of terbium, turns out to be about 1/3 of that in dysprosium.

If it is assume that the values of the sf exchange integral, $\mathcal{J}$, and the density of states are same as those of dysprosium, the numerical estimation of eqn (4.21) of Part I can be performed also for terbium. Because of the uncertainties in various parameters and rough approximations made in the calculation, the estimated value is only a tentative one, but the calculated value of $W_o = W_{-3/2,-1/2}/T \sim 1\times10^4 \text{sec}^{-1}\text{K}^{-1}$ is quite in good agreement with the experimental value, $4.58\times10^3 \text{sec}^{-1}\text{K}^{-1}$.

Because the relaxation probability due to this process is proportional to $\omega^2_{m,m+1}(I-m)(I+m+1)T$, the calculated decay curves

expected from this relaxation process are entirely in agreement with the experimental data as shown in previous section, if we choose an approximate value for the parameter W_o.

Thus it is concluded that the relaxation process via spin-waves through 4f hyperfine interactions and sf exchange interactions is the main one for the nuclear spin-lattice relaxation in ferromagnetic terbium metal just as in dysprosium.metal.

IV 3. Spin-Spin Relaxation

In Sec. IV-3 of Part I, we calculated the contribution from the spin-lattice relaxation to T_2, the transverse relaxation time or the time constant of the decay of the echo envelope, but in that calculation we neglected the contribution from the Suhl-Nakamura interaction[8] to T_2. Because the natural abundance of ^{159}Tb is 100% and is four times of that of ^{163}Dy, we can not probably neglect the contribution from the Suhl-Nakamura interaction to T_2. Then, the equation (4.25) of Part I may be written by

$$1/T_2 = W_{m,m+1} + \frac{1}{2}(W_{m+1,m+2} + W_{m-1,m}) + 1/(T_2^*)_{m,m+1} , \qquad (4.5)$$

where $1/(T_2^*)$ is the contribution from the Suhl-Nakamura interaction to T_2 and is independent of absolute temperature. At low temperature, $W_{m\rightarrow m+1}$ is not equal to $W_{m+1\rightarrow m}$, then the equation (4.5) turns out

$$1/T_2 = (W_{m+1\rightarrow m+2} + W_{m\rightarrow m+1} + W_{m+1\rightarrow m} + W_{m\rightarrow m-1}) + 1/(T_2^*)_{m,m+1} . \qquad (4.6)$$

Using the value of W_o, we calculated the value of the contribution from the spin-lattice relaxation to T_2 by the equation (4.6). The results is shown by solid curves in Fig. 9. We evaluated

the contribution from the Shul-Nakamura interaction to T_2 from the gaps between these solid curves and the experimental plots. The results are $1/(T_2^*)_{-1/2,+1/2} \simeq 1\times10^4 sec^{-1}$ and $1/(T_2^*)_{\pm1/2,\pm3/2} \simeq 2\times10^4 sec^{-1}$.

Sherrington[27] have calculated the spin-spin relaxation time in ferromagnetic terbium metal due to the Suhl-Nakamura mechanism. The calculated values are $1/(T_2^*)_{-1/2,+1/2} \simeq 4\times10^5 sec^{-1}$ and $1/(T_2^*)_{\pm1/2,\pm3/2} \simeq 2.7\times10^5 sec^{-1}$. These values are larger than the experimental values and the calculated result that $1/(T_2^*)$ of the center line is larger than those of the outer lines, is opposite to our experimental results. As already described in Sec. III-1, each line has a width of about ten MHz, which is much larger than the width expected from T_2^*. The resonance lines therefore are inhomogeneously broadened and the spin-spin relaxation time due to I·I coupling will become much longer than in the homogeneous line. Because the spins having the resonance frequencies within the range γH_1 (H_1 is the enhanced rf amplitude) contribute the observed resonance, and the rf pulse of the 1 μsec corresponds 90° pulse, about 1/10 of the whole number of spins contribute to the resonance. Therefore it can be understood that T_2^* becomes longer by about one order of magnitude as compared to the theoretical value calculated for a homogenious line. But it is not known why $1/(T_2^*)$ of the side two lines is about the twice of that of the center line. Experiments by more perfect crystal should be needed to obtain the more accurate value of $1/(T_2^*)$ arising from I·I coupling to compare with the theoretical value.

Acknowlegements

The author would like to express his gratitude for the continuous guidance and encouragement of Professor J. Itoh, under whose direction this work was performed. He also wish to thank Dr. S. Kobayashi on the guidance in initiating this work.

Appendix. The Solution of Rate Equations for the Spin-Lattice Relaxation at Low Temperature.

Functional forms of the spin-lattice relaxation decay in the case of the high-temperature approximation have been calculated in Appendix of Part I under the assumption that the nuclear energy levels are unequally spaced and the transition probability depends upon the spacing of the nuclear levels. In the case of ^{159}Tb, however, the Zeeman energy is so large that the high-temperature approximation cannot be applied. At low temperature. the ratio of $W_{m\rightarrow m+1}$ to $W_{m+1\rightarrow m}$ cannot be approximated to be unity but is

$$W_{m\rightarrow m+1} / W_{m+1\rightarrow m} = e^{\left\{-E(m+1)+E(m)\right\}/kT}, \qquad (A.1)$$

where $E(m)$ is the nuclear energy of $I_z=m$. In this Appendix, functional forms of the spin-lattice relaxation decay at low temperature are calculated under the assumption that the transition probability, $W_{m+1\rightarrow m}$, is proportional to $\omega^2_{m,m+1}\left\{ I(I+1)-m(m+1)\right\}$ and the $W_{m\rightarrow m+1}$ is equal to $W_{m+1\rightarrow m}\exp\left\{ E(m)-E(m+1)\right\}/kT$.

The numerical solution of the secular equation for λ_j, in the case of ^{159}Tb, turns out, at 4.22K,

$$\lambda_j / W_{-1/2\rightarrow -3/2} = 0.9304,\ 3.08000,\ 6.9281 \qquad (A.2)$$

for j=1, 2, and 3, respectively. Hence, numerical solutions of the relative decay curves of the stimulated echo signal at 4.22K are given by following equations.

For the transition $+3/2 \rightleftarrows +1/2$

$$a_{+3/2}=0.0384\exp(-\lambda_1 t)+0.5315\exp(-\lambda_2 t)+1.4301\exp(-\lambda_3 t)$$

For the transition $+1/2 \rightleftarrows -1/2$

$$a_{+1/2}=0.1314\exp(-\lambda_1 t)+0.3238\exp(-\lambda_2 t)+1.5447\exp(-\lambda_3 t)$$

For the transition $-1/2 \rightleftarrows -3/2$

$$a_{-1/2}=0.5632\exp(-\lambda_1 t)+1.1542\exp(-\lambda_2 t)+0.2827\exp(-\lambda_3 t).$$

Here, λ_j and $a_m(t)$ are already presented in Appendix of Part I.

At 1.35K,

$$\lambda_j/W_{-1/2\longrightarrow -3/2}=0.9112,\ 2.9726,\ 6.6451 \qquad (A.3)$$

for j=1, 2, and 3, respectively.

$$a_{+3/2}= 0.03119\exp(-\lambda_1 t)+0.5268\exp(-\lambda_2 t)+1.4420\exp(-\lambda_3 t)$$

$$a_{+1/2}= 0.1287\exp(-\lambda_1 t)+0.3362\exp(-\lambda_2 t)+1.5346\exp(-\lambda_3 t)$$

$$a_{-1/2}= 0.5833\exp(-\lambda_1 t)+1.1361\exp(-\lambda_2 t)+0.2806\exp(-\lambda_3 t).$$

The difference between the results at 4.22K and those at 1.35K is still small, but the numerical solution of secular equation for λ_j at 0.1K gives

$$\lambda_j/W_{-1/2\longrightarrow -3/2}=0.9278,\ 2.0853,\ 3.7414. \qquad (A.4)$$

The decay curves at 0.1K are much different from those at 1.35K or 4.22K. Hence, the decay measurement at still lower temperature seems interesting.

Figure Captions

Fig. 1. Block diagram of the spin echo apparatus in UHF range.

Fig. 2. Lighthouse-tube reentrant cavity oscillator.

Fig. 3. Sample cavity.

Fig. 4. Typical stimulated echo of the 3794MHz line of ^{159}Tb in ferromagnetic terbium metal at 1.35K. The pulses have a width 1μsec. τ=5μsec. and T=20μsec. The primary echo at 2 corresponding to twin pulses at 0 and is not observed, because of the PIN diode is switched off by the gated pulse.

Fig. 5. The line shapes of NMR lines of ^{159}Tb in ferromagnetic terbium metal.

Fig. 6. Comparison of experimental and theoretical spin-lattice relaxation decays for all three resonance lines of ^{159}Tb in ferromagnetic terbium metal. Plots are the experimental values at 1.35K, while the solid curves are the calculated ones using $W_{-1/2\rightarrow -3/2}=6.18\times10^{3}\,\mathrm{sec}^{-1}$.

Fig. 7. Plots of the observed stimulated echo amplitudes for the resonance line of ^{159}Tb at 2447MHz at 1.35K, 2.58K, and 4.22K.

Fig. 8. Plots of the observed stimulated echo amplitudes with different values of for the center line of ^{159}Tb resonance at 3120MHz at 1.35K.

Fig. 9. Plots of the observed T_2 values for all three resonance lines of ^{159}Tb in ferromagnetic terbium metal. The solid curves are the contributions from the spin-lattice relaxation.

Figure Captions (continued)

Fig. 10. Comparison of the 3120MHz line of ^{159}Tb in ferromagnetic pure terbium metal and in ferromagnetic Tb_{90}-Y_{10} alloy.

Fig. 11. The spin-wave spectrum of terbium along symmetry directions in the Brilloun zone obtained by Møller and Houmann by inelastic neutron scattering at 90K.

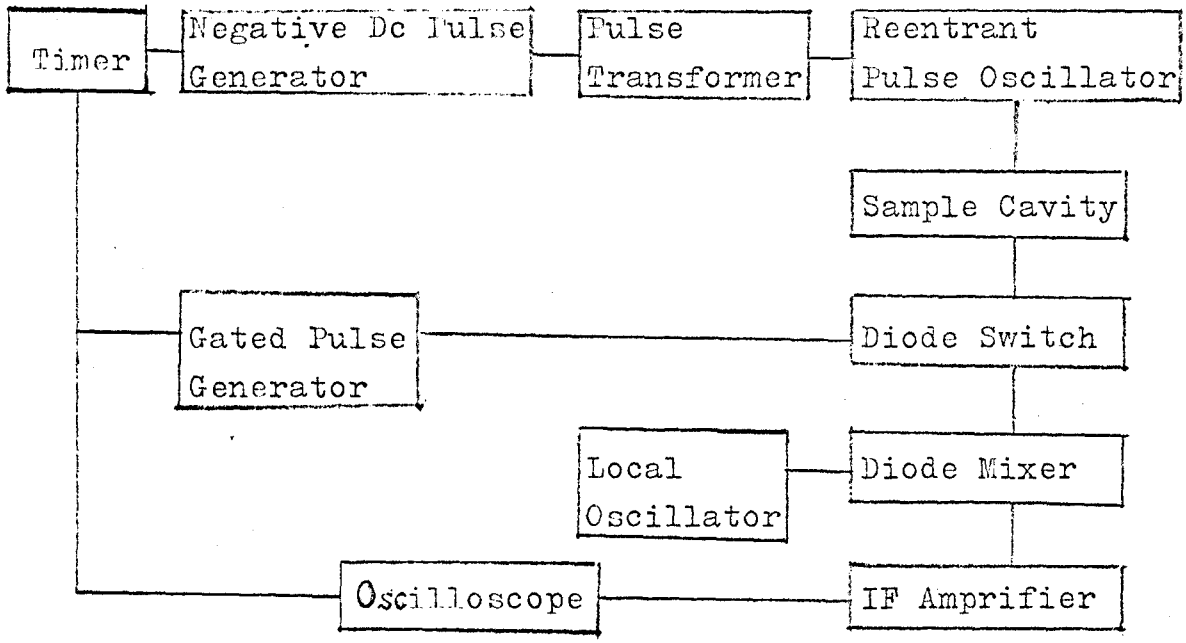
Timer
Negative Dc Pulse Generator
Pulse Transformer
Reentrant Pulse Oscillator
Sample Cavity
Gated Pulse Generator
Diode Switch
Local Oscillator
Diode Mixer
Oscilloscope
IF Amprifier

Fig. 1

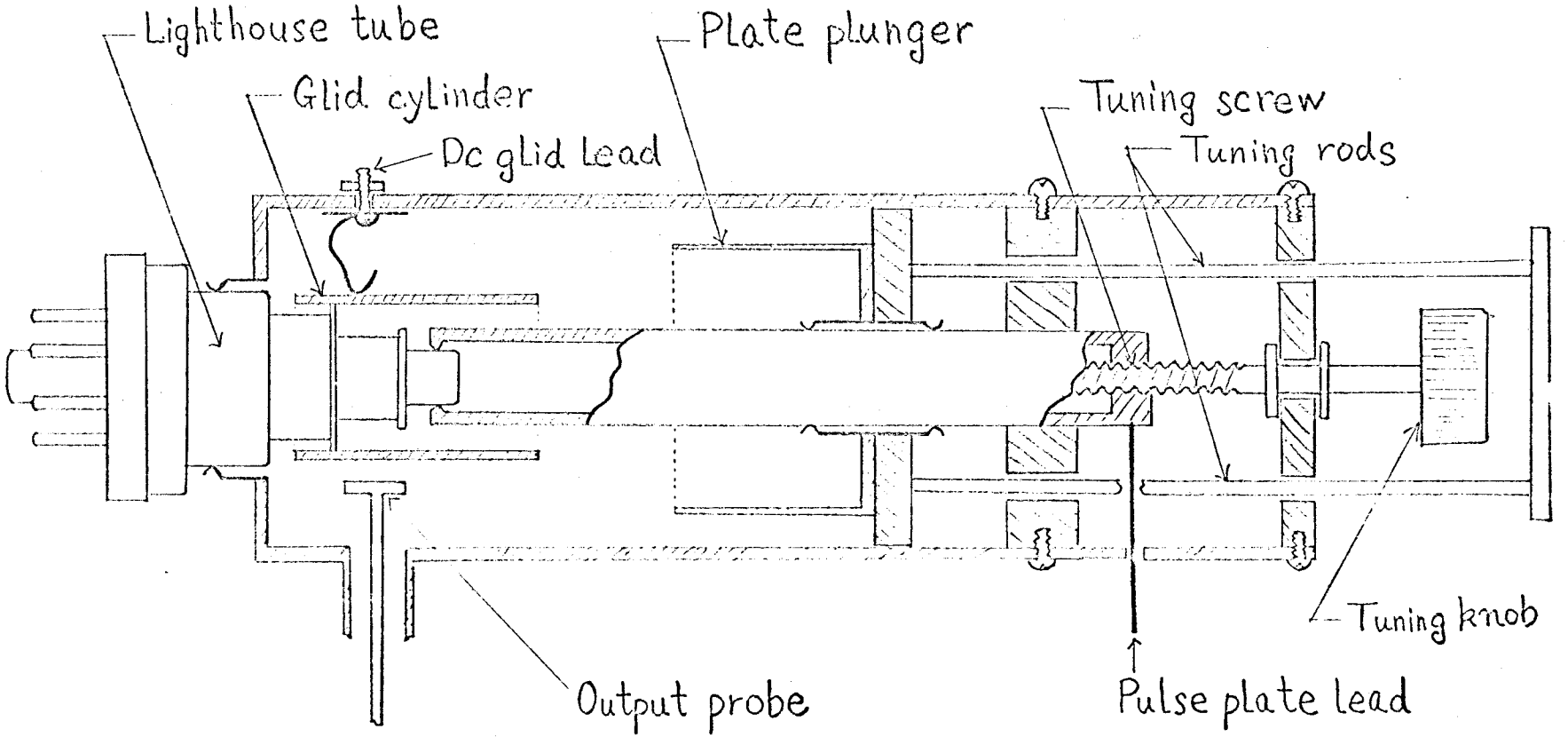
Lighthouse tube
Glid cylinder
Dc glid lead
Plate plunger
Tuning screw
Tuning rods
Tuning knob
Output probe
Pulse plate lead

Fig. 2

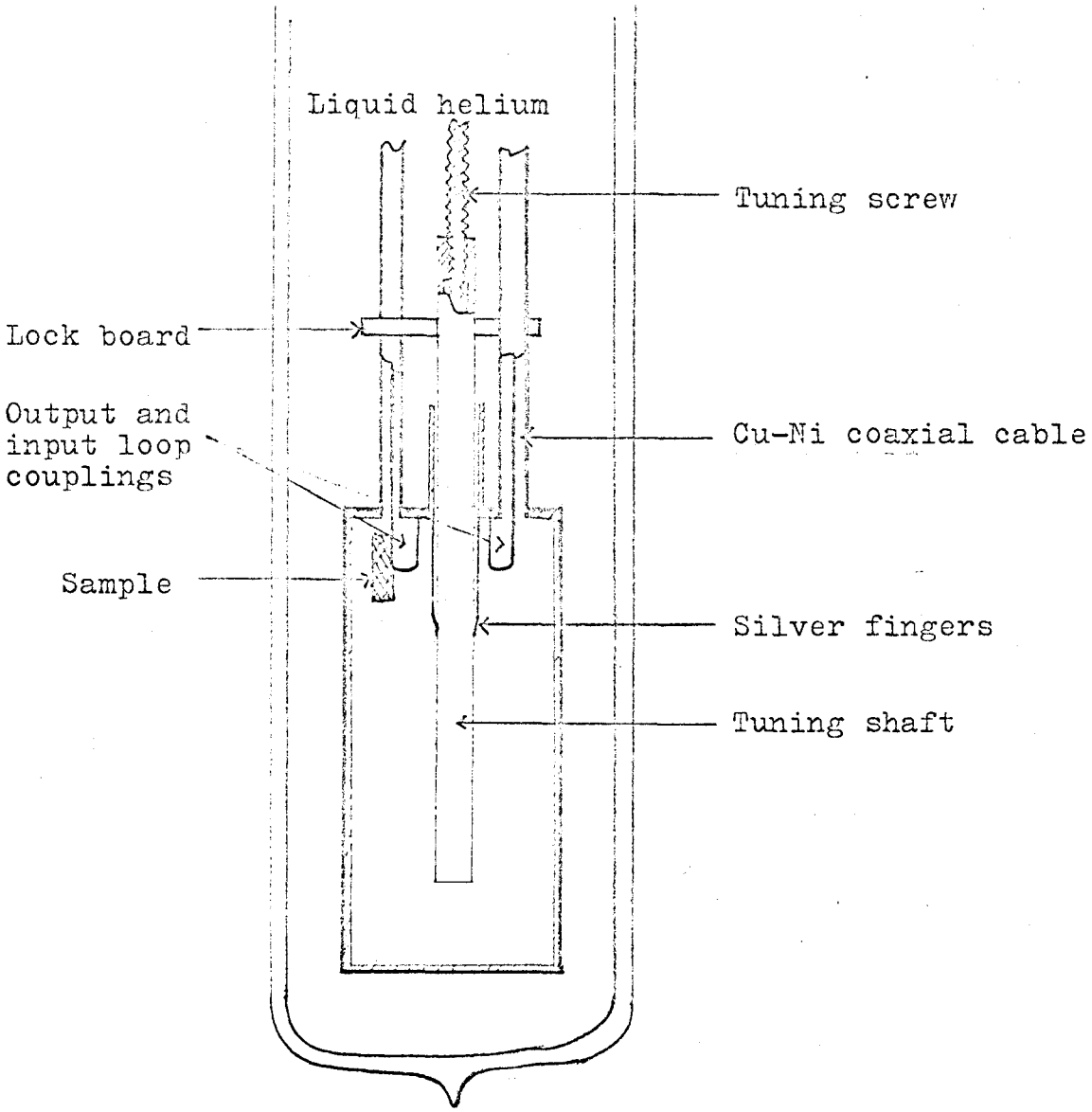
Liquid helium
Tuning screw
Lock board
Output and
input loop
couplings
Cu-Ni coaxial cable
Sample
Silver fingers
Tuning shaft

Fig. 3

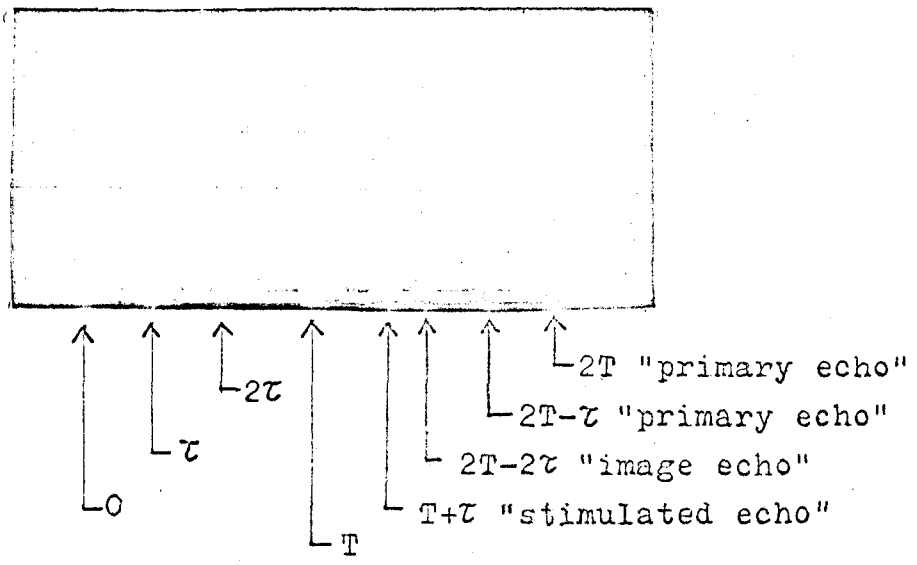
0
τ
2τ
T
T+τ "stimulated echo"
2T-2τ "image echo"
2T-τ "primary echo"
2T "primary echo"

Fig. 4

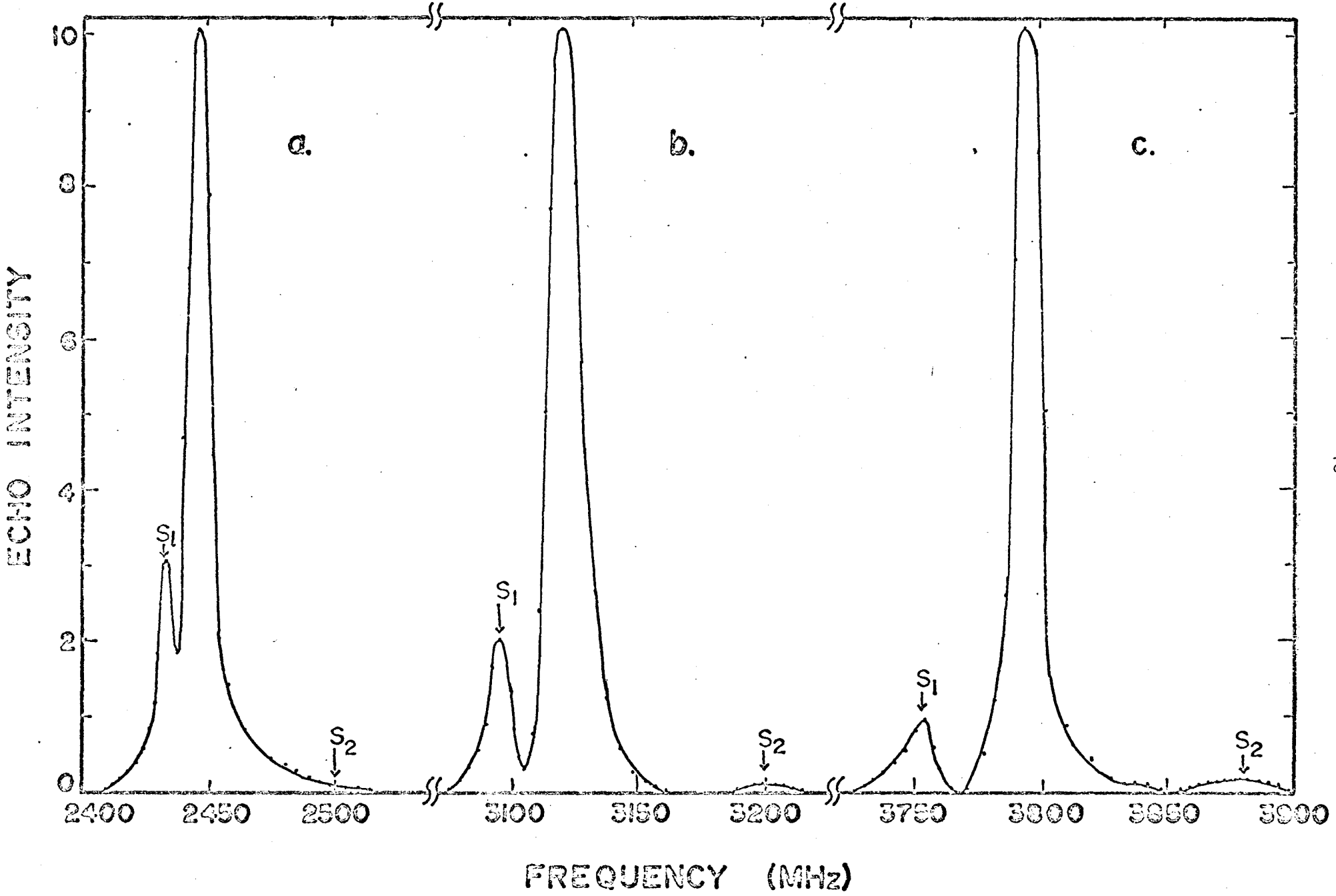
ECHO INTENSITY
FREQUENCY (MHz)
a.
b.
c.
S1
S2
0
2
4
6
8
10
2400
2450
2500
3100
3150
3200
3750
3800
3850
3900

Fig. 5

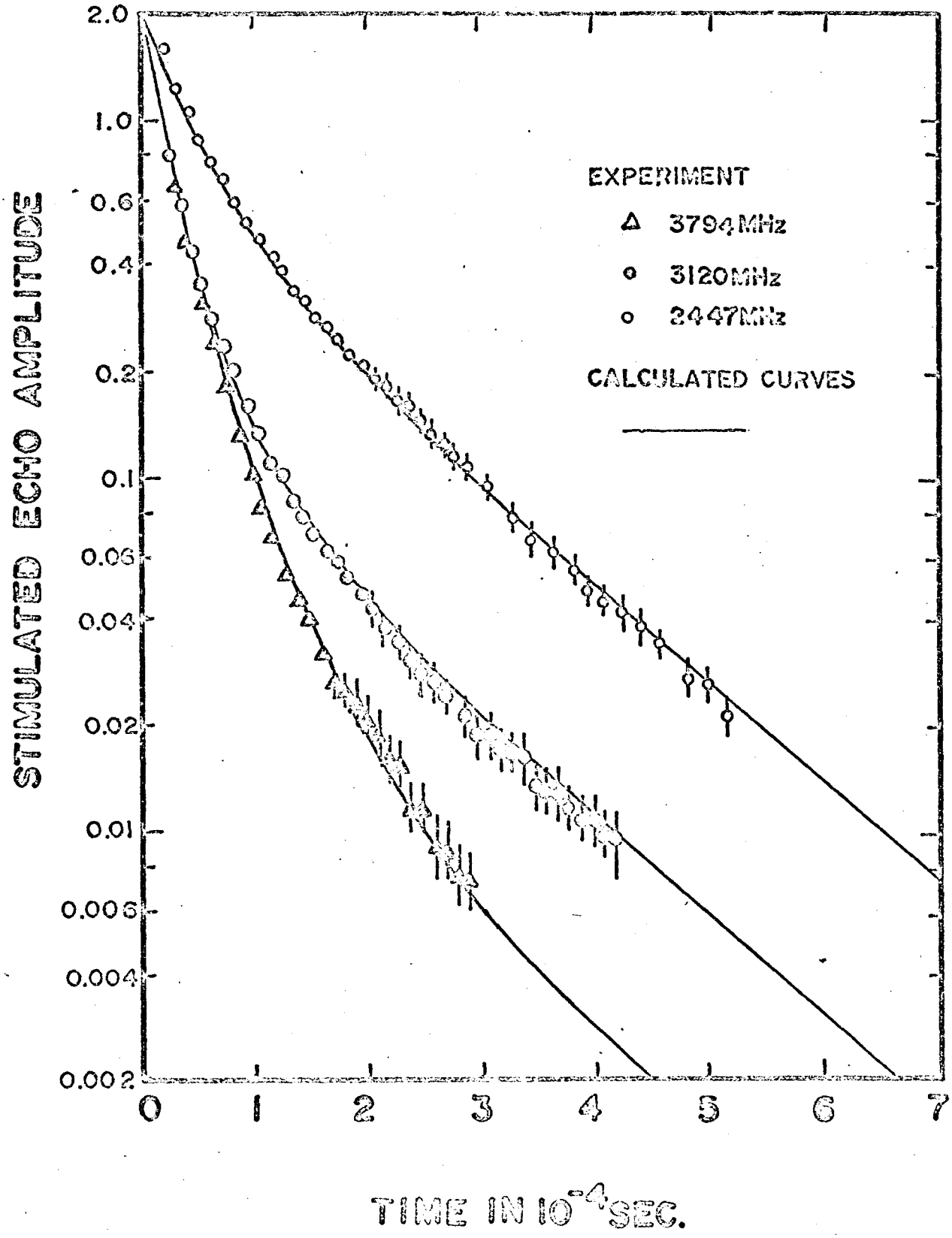
STIMULATED ECHO AMPLITUDE
2.0
1.0
0.6
0.4
0.2
0.1
0.06
0.04
0.02
0.01
0.006
0.004
0.002
0
1
2
3
4
5
6
7
TIME IN 10^{-4} SEC.
EXPERIMENT
Δ 3794MHz
o 3120MHz
o 2447MHz
CALCULATED CURVES

Fig. 6

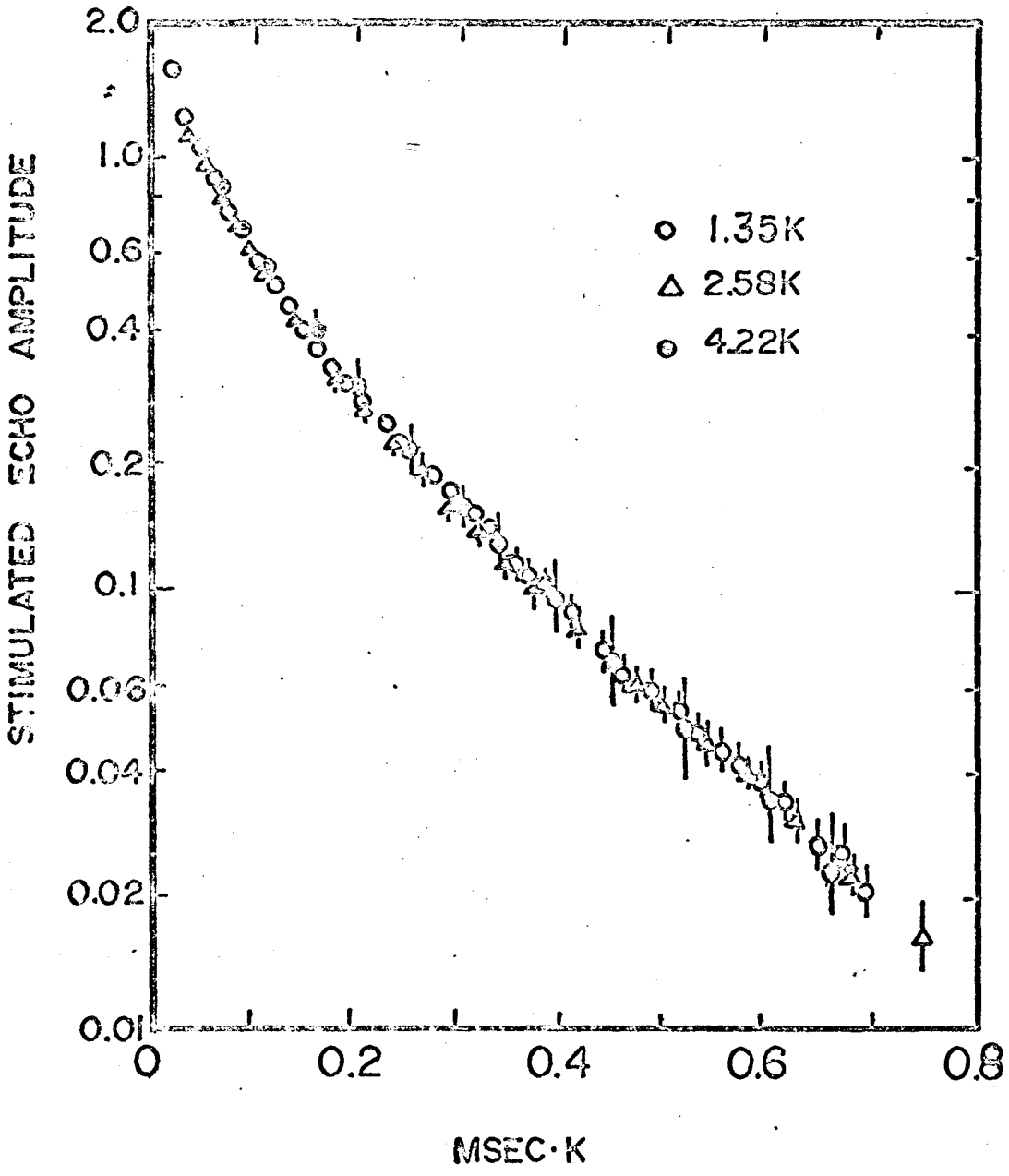
STIMULATED ECHO AMPLITUDE
2.0
1.0
0.6
0.4
0.2
0.1
0.06
0.04
0.02
0.01
0
0.2
0.4
0.6
0.8
MSEC·K
1.35K
2.58K
4.22K

Fig. 7

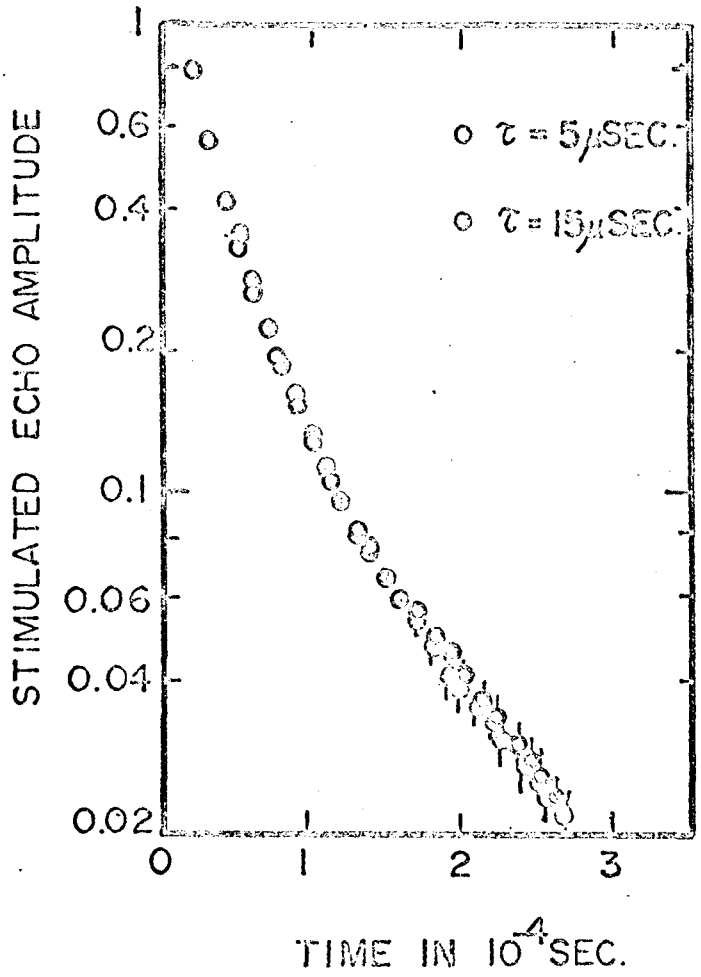
STIMULATED ECHO AMPLITUDE
1
0.6
0.4
0.2
0.1
0.06
0.04
0.02
0
1
2
3
TIME IN 10^{-4} SEC.
o τ = 5μSEC.
o τ = 15μSEC.

Fig. 8

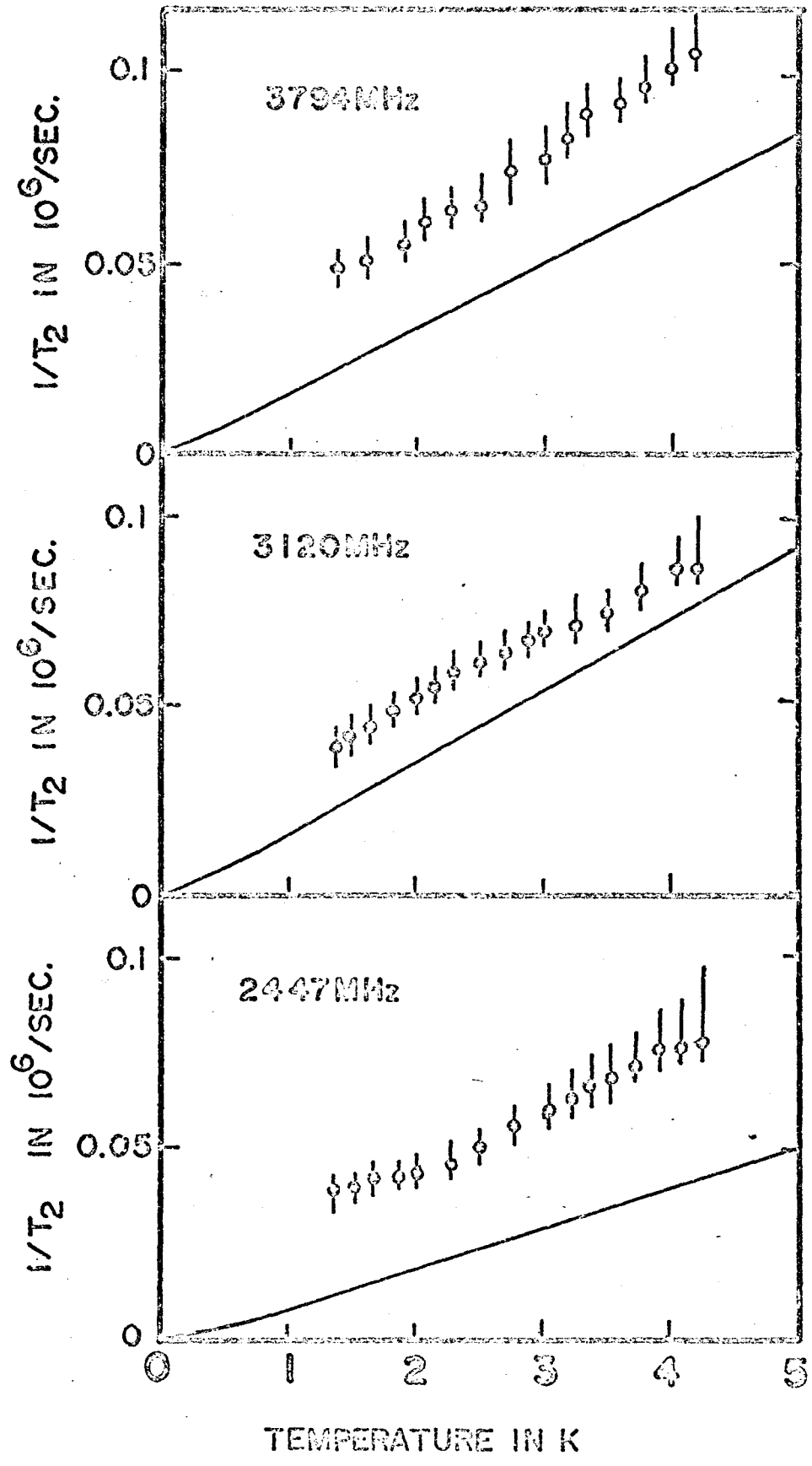
3794MHz
3120MHz
2447MHz
0.1
0.05
0
1/T2 IN 10^6/SEC.
0
1
2
3
4
5
TEMPERATURE IN K

Fig. 9

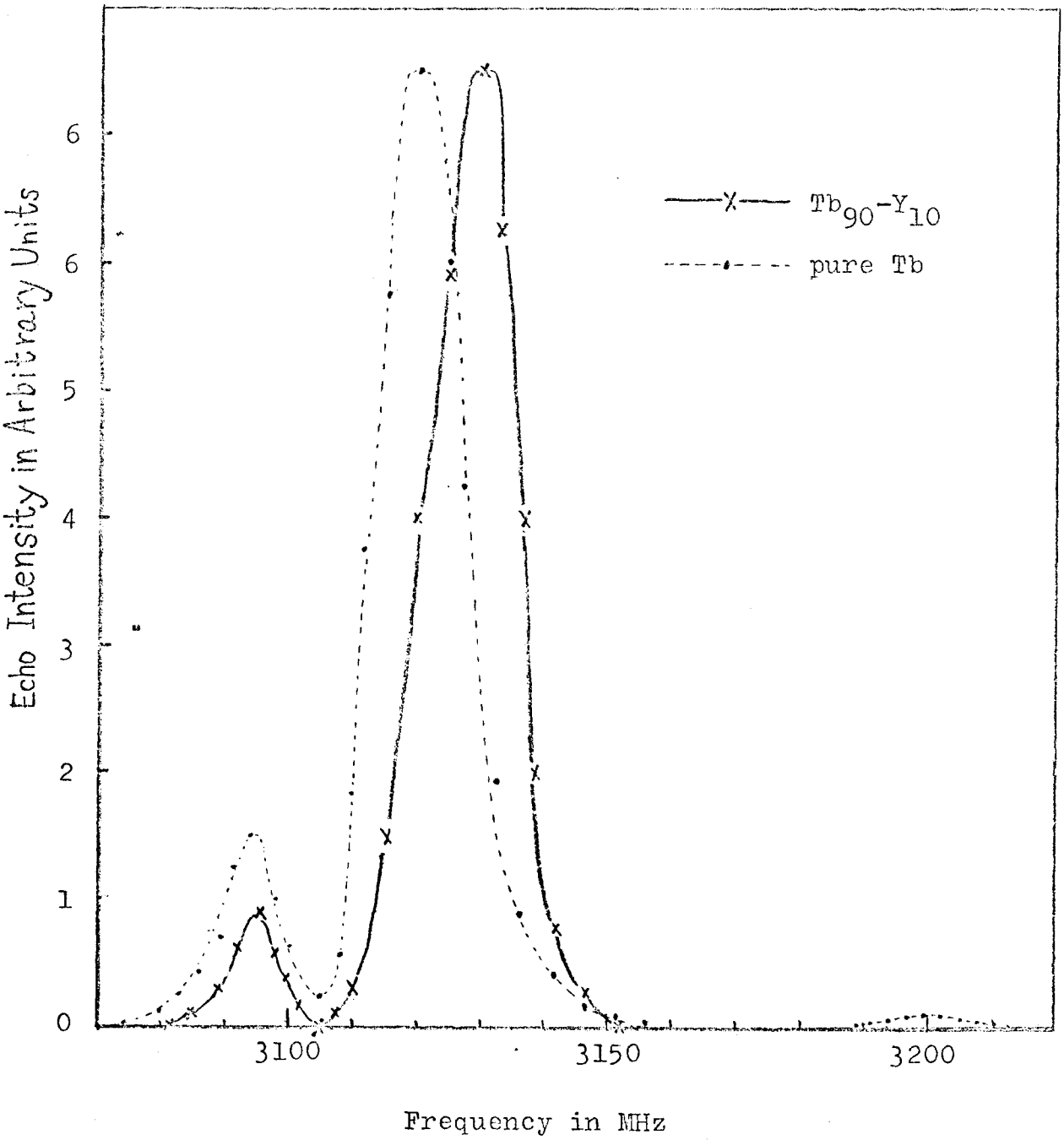
Echo Intensity in Arbitrary Units
0
1
2
3
4
5
6
6
3100
3150
3200
Frequency in MHz
$Tb_{90}-Y_{10}$
pure Tb

Fig. 10

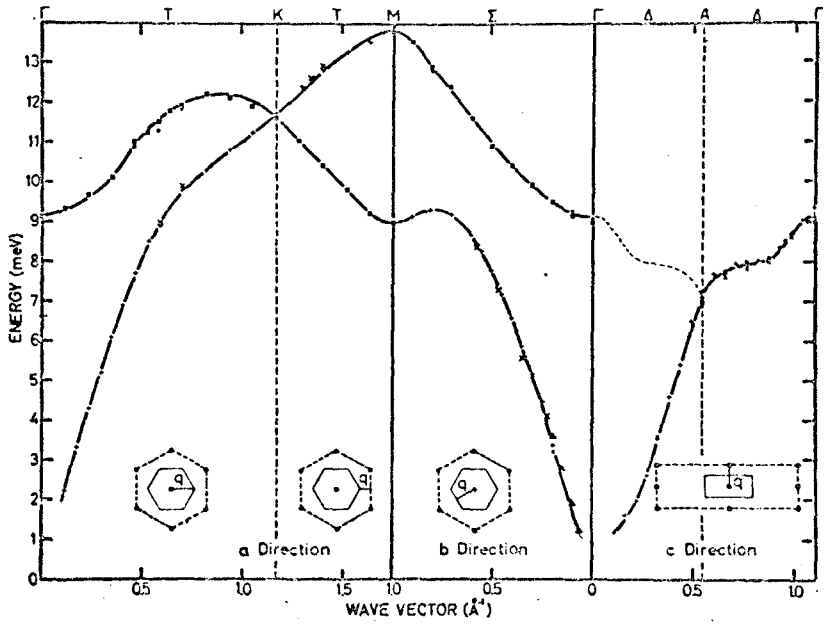
Γ T K T M Σ Γ Δ A Δ Γ
ENERGY (meV)
WAVE VECTOR (Å⁻¹)
a Direction
b Direction
c Direction
q

Fig. 11

Reference

1) M. Weger: Phys. Rev. 128 (1962) 1505.

2) E. C. Heltemes and C. A. Swenson: J. Chem. Phys. 35 (1961) 1264

O. V. Lounasmaa and P. R. Roach: Phys. Rev. 128 (1962) 622.

3) J. C. Woolum and A. J. Bearden: Phys. Rev. 142 (1966) 143.

4) J. Herve and P. Veillet: CR Acad. Sci. 252 (1961) 99.

5) S. Kobayashi: Thesis, Osaka Univ. 1967.

6) E. L. Harn: Phys. Rev. 80 (1950) 580.

7) N. Bloembergen, M. M. Purcell and R. V. Pound: Phys. Rev. 73 (1948) 679.

8) H. Suhl: Phys. Rev. 109 (1958) 606; J. Phys. Radium 20 (1959) 333

T. Nakamura: Progr. Theor. Phys. 20 (1958) 542.

9) R. E. Walstedt: Phys. Rev. Letters 19 (1967) 146; ibid., 816.

10) B. Bleaney: J. appl. Phys. 34 (1963) 1024.

11) J. Kondo: Phys. Soc. Japan 16 (1961) 1690; ibid., 17 (1962) 413.

12) M. Teraoka, N. Sano, and J. Itoh: to be published.

13) B. Bleaney: Proceedings The Third Quantum Electronics Conference. Dunod, Paris. (1964)

14) J. Itoh, S. Kobayashi, and N. Sano: J. appl. Phys. 39 (1968) 1325.

15) W. C. Koehler, H. R. Child, E. O. Wollan, and J. W. Cable: J. appl. Phys. 34 (1963) 1335.

16) F. J. Darnell: Phys. Rev. 132 (1963) 1098.

17) M. K. Wilkinson, H. R. Child, W. C. Koehler, J. W. Cable, and E. O. Wollan: J. Phys. Soc. Japan 17 BIII, (1962) 27; Phys. Rev. 131 (1963) 922.

Reference (continued)

18) B. C. Gerstein, F. J. Jelinek, and F. H. Spedding: Phys. Rev. Letters 8 (1962) 425.

19) A. Abragam and B. Bleaney: Electron Paramagnetic Resonance of Transition Ions, (Claredon Press, 1970), p301.

20) R. M. Sternheimer: Phys. Rev. 84 (1951) 244.

21) F. W. deWette: Phys. Rev. 123 (1961) 103.

22) D. L. Uhrich and R. G. Barnes: Phys. Rev. 164 (1967) 428.

23) A. Narath: Phys. Rev. 179 (1969) 359.

24) H. B. Møller and J. C. G. Houmann: Phys. Rev. Letters 16 (1966) 737.

25) D. A. Gooding: J. Phys. C (Proc. Phys. Soc.) 1 (1968) 125. M. S. S. Brooks, D. A. Gooding, and H. I. Ralph: J. Phys. C (Proc. Phys. Soc.) 1 (1968) 1596.

26) S. C. Keeton and T. L. Loucks: Phys. Rev. 168 (1968) 672.

27) D. Sherrington: J. Phys. C (Proc. Phys. Soc.) 1 (1968) 748.